NRF2 activation reprogrammes defects in oxidative metabolism to restore macrophage function in COPD

Title: NRF2 activation reprogrammes defects in oxidative metabolism to restore macrophage function in COPD

Authors: Eilise M. Ryan[1], Pranvera Sadiku[1], Patricia Coelho[1,] Emily R. Watts[1], Ailiang Zhang[1], Andrew J.M. Howden[2], Manuel A. Sanchez-Garcia[1], Martin Bewley[3], Joby Cole[3], Brian J. McHugh[1], Wesley Vermaelen[4], Bart Ghesquiere[4], Peter Carmeliet[5,6,7], Giovanny Rodriguez Blanco[8], Alex Von Kriegsheim[8], Yolanda Sanchez[9], William Rumsey[9], James F. Callahan[9], George Cooper[1], Nicholas Parkinson[10], Kenneth Baillie[10], Doreen A. Cantrell[2] , John McCafferty[11], Gourab Choudhury[11], Dave Singh[12], David H. Dockrell[1], Moira K.B. Whyte[1*]†, Sarah R. Walmsley[1*]†.

Affiliations:

[1]University of Edinburgh Centre for Inflammation Research, The Queen's Medical Research Institute, University of Edinburgh, Edinburgh, UK

[2]Division of Cell Signalling and Immunology, University of Dundee, Dundee, DD1 5EH, UK

[3]Department of Infection, Immunity and Cardiovascular Disease, University of Sheffield, Sheffield, UK

[4]Metabolomics Expertise Centre, VIB-KU Leuven Centre for Cancer Biology, Leuven 3000, Belgium

[5] Laboratory of Angiogenesis and Vascular Metabolism, Centre for Cancer Biology, VIB, Department of Oncology, Leuven Cancer Institute, KU Leuven, Leuven 3000, Belgium

[6]Laboratory for Translational Breast Cancer Research, Department of Oncology, KU Leuven, Leuven 3000, Belgium

[7]State Key Laboratory of Ophthalmology, Zhongshan Ophthalmic Centre, Sun Yat-Sen University, Guangzhou, Guangdong, P.R. China

[8] Cancer Research UK Edinburgh Centre, Institute of Genetics and Cancer, University of Edinburgh, Edinburgh, UK

[9] GlaxoSmithKline Research & Development, Collegeville, PA 19426, United States

[10] MRC Human Genetics Unit, Institute of Genetics and Molecular Medicine, University of Edinburgh, Edinburgh EH4 2XU, UK

[11]NHS Lothian, Respiratory Medicine, Edinburgh, UK

[12]Division of Infection, Immunity and Respiratory Medicine, University of Manchester, Manchester, UK

†Contributed equally to this work

*To whom correspondence should be addressed: Professors Sarah Walmsley and Moira Whyte, University of Edinburgh Centre for Inflammation Research, The Queen's Medical Research Institute, Edinburgh BioQuarter, 47 Little France Crescent, Edinburgh. EH16 4TJ . Tel: +44 (0)131 242 9100. Email: sarah.walmsley@ed.ac.uk and moira.whyte@ed.ac.uk

Author Contributions E.M.R., P.S., P.C.[1], A.Z., A.H., J.C., W.V., B.G., G.R.B, B.J.McH. and G.C.[1] performed the research. E.M.R., J.M.C, G.C.[11] and D.S. recruited

patient cohorts and performed bronchoscopy. E.R.W., M.S.G., M.B., P.C.[5,6,7] and D.C. contributed technical expertise. Y.S., W.R. and J.F.C. provided the GSK drug compound and contributed to experimental design. E.M.R., P.S., A.V.K., N.P, K.B., D.H.D, M.K.B.W and S.R.W. provided scientific interpretation of the data. E.M.R., M.K.B.W and S.R.W designed the research and wrote the manuscript.

Short running head: NRF2 rescues macrophage metabolism in COPD

9.13 COPD: Pathogenesis

Word count: 4049

This article has an online data supplement, which is accessible from this issue's table of content online at **www.atsjournals.org**

Abstract

Rationale: COPD (Chronic Obstructive Pulmonary Disease) is a disease characterized by persistent airway inflammation and disordered macrophage function. The extent to which alterations in macrophage bioenergetics contribute to impaired antioxidant responses and disease pathogenesis has yet to be fully delineated.

Objectives: Through the study of COPD alveolar (AM) and peripheral monocyte-derived (MDM) macrophages, we sought to establish if intrinsic defects in core metabolic processes drive macrophage dysfunction and redox imbalance.

Methods: AM and MDM from COPD and healthy donors underwent functional, metabolic and transcriptional profiling.

Results: We observe that AM and MDM from COPD donors display a critical depletion in glycolytic and mitochondrial respiration derived energy reserves and an over reliance on glycolysis as a source for ATP, resulting in reduced energy status. Defects in oxidative metabolism extend to an impaired redox balance associated with defective expression of the NADPH generating enzyme, malic enzyme 1, a known target of the anti-oxidant transcription factor NRF2. Consequently, selective activation of NRF2 resets the COPD transcriptome, resulting in increased generation of TCA cycle intermediaries, improved energetic status, favorable redox balance and a recovery of macrophage function.

Conclusion: In COPD an inherent loss of metabolic plasticity leads to metabolic exhaustion and reduced redox capacity which can be rescued by activation of the NRF2

pathway. Targeting these defects, via NRF2 augmentation, may therefore present an attractive therapeutic strategy for the treatment of the aberrant airway inflammation described in COPD.

Word count: 233

Introduction

COPD is the third leading cause of death globally. To date we have no therapies which significantly alter the course of this debilitating disease. The histological hallmark of COPD is persistent inflammation of the airways, resulting in airflow limitation, measured by a decline in forced expiratory volume in 1 second (FEV1), chronic bronchitis and emphysema. This inflammation persists in people with COPD, even following smoking cessation[1].

It has long been established that macrophages play a major role in the pathogenesis of COPD. Alveolar macrophages are present in high numbers in the airways and airway secretions of patients with COPD, where their abundance correlates directly with disease severity[2]. Despite this abundance, patients with COPD experience high rates of infection, with pathogenic bacteria in the lower airways strongly associated with exacerbation frequency and increased inflammation[3]. This major disconnect, whereby excessive cellular inflammation results in ineffective immunity, is now understood to be largely driven by macrophage dysfunction. Work from our group and others has previously shown that COPD macrophages have defective phagocytosis of bacteria that colonize the lungs in COPD, such as non-typeable *Haemophilus influenzae* and *Streptococcus pneumoniae*[4,5,6,7]. Macrophage dysfunction also extends to impaired inflammation resolution, with failure to efferocytose apoptotic cells also described[8]. In conjunction with impaired macrophage internalization rates, macrophages in COPD also produce molecules known to induce pulmonary tissue damage including matrix metalloproteinases (MMPs)[9,10] and reactive oxygen species (ROS)[11]. ROS, in particular,

3

have been linked to mitochondrial dysfunction in COPD[12]. Thus, in COPD, macrophages demonstrate functional responses that are ineffective and skew the balance towards "self-injury" in the lung. Despite these well characterized defects in macrophage function, the mechanisms that drive this aberrant behavior remain poorly defined[7,13,14]. Therefore, through the study of macrophages isolated from the airways [Alveolar Macrophages (AM)] and peripheral blood [Monocyte-derived macrophages (MDM)] of COPD and healthy donors we sought to delineate the intrinsic processes that promote macrophage dysfunction in COPD. We demonstrate that in COPD, alveolar and monocyte-derived macrophages share an inherent defect in efferocytosis and phagocytosis, driven by the loss of oxidative and glycolytic reserve capacity and impaired metabolic plasticity. Reduced expression of the NADPH generating enzyme malic enzyme 1, recapitulates these metabolic defects and results in a reduction in redox buffering capacity and impaired efferocytosis. By activating the anti-oxidant transcription factor NRF2, we were able to rescue ME1 expression and restore metabolic plasticity and function in COPD macrophages. Some of the results of this study have been previously reported in the form of abstracts[15,16,17,18].

Materials and Methods:

Macrophage donors: COPD and healthy donors underwent bronchoscopy and venesection. Patient demographics are outlined in Table 1. Written informed consent was obtained in accordance with local ethics approval, as detailed in the online supplement.

Cell Culture: Alveolar macrophages were isolated from BAL as previously described[19], with 93-97% purity as assessed by Cytospin. MDM were differentiated from peripheral blood mononuclear cells isolated via discontinuous plasma-Percoll gradients (Sigma-Aldrich), for 14 days in culture. For Seahorse MDM experiments, monocytes were isolated using the Miltenyi Biotec Pan-Monocyte Isolation kit then plated into low-adherence flasks (Corning) for culture. THP-1 cells were differentiated to macrophages by treating with 100 nM PMA for 3 days, then rested for 3 days prior to assay. Cells were treated with 0.065 µM KI-696, a selective inhibitor of the KEAP1–NRF2 interaction or vehicle control x16 hours prior to assays. All cells were cultured in RMPI 1640 (Sigma-Aldrich) with 10% heat inactivated FCS (Gibco).

Functional assays: Bacterial internalisation assays were performed as previously described[7], using opsonized Serotype 14 *S. pneumoniae* (National Collection of Type Cultures 11902). For efferocytosis assays, neutrophils isolated via Percoll-gradient were stained with a PKH26 labelling kit, as per manufacturers guidelines (Sigma-Aldrich), and cultured for 20h in RMPI 1640. Apoptotic neutrophils (70-80% apoptotic verified by Annexin-V-Topro3 staining) were added to macrophages at MOI 5:1, with ice control, for 90 minutes before vigorously washing and removal for analysis on a Becton Dickinson FACS Calibur flow cytometer[20].

Quantification and Statistical Analysis: Data represents mean ± SEM. Statistical parametric analyses were performed following confirmation of normal distribution of the data via D'Agostino-Pearson normality tests. All statistical tests were performed with Prism 8 software (GraphPad Software) using unpaired t-tests, paired t-tests, one-way or two-way ANOVA with Sidak's multiple comparisons test, Pearsons 's correlation.

Wilcoxon matched paired signs rank test, Mann Whitney and Kruskal Wallis with Dunns multiple comparison tests were performed for nonparametric or n$\leq$ 6 data. *P $\leq$0.05, **P$\leq$0.01, ***P$\leq$0.001.

Results

Correlation of defective macrophage efferocytosis with phagocytosis in COPD.

To study macrophage efferocytosis and phagocytosis we recruited COPD patients with mild (14 patients, 27%) moderate (26 patients, 50%), severe (11 patients, 21%) and very severe disease (1 patient, 2%), who were free from exacerbation for $\geq$8 weeks minimum and age matched ($\pm$ 8 years; mean age) with healthy controls (Table 1). In line with disease status, forced expiratory volume in one second (FEV$_1$) was significantly lower in COPD donors and 43/52 (82%) of COPD donors had COPD Assessment test scores (CAT scores) $\geq$10, in keeping with severe symptoms.

Alveolar macrophages (AM) and peripheral monocyte-derived macrophages (MDM) were compared to interrogate intrinsic and extrinsic (niche dependent) factors impacting on macrophage function. Both AM and MDM isolated from patients with COPD demonstrated defective phagocytosis of live opsonised S14 *S.pneumoniae* (Fig. 1A-B), and efferocytosis of PKH26 labelled apoptotic neutrophils compared to healthy controls (HC) (Fig. 1C-D), as previously described[7,20]. Rates were lowest in current smokers across both processes, as expected[21], but macrophage dysfunction did not recover in COPD patients who were no longer active smokers (Fig. 1A-D). To establish if there was a direct clinical read out of impaired efferocytosis in COPD, we performed correlation analysis of

6

macrophage efferocytosis against FEV_1. There was a significant relationship observed

between macrophage efferocytosis and FEV_1 % predicted (Actual Donor FEV1 as a % of

their predicted FEV1, based on height and age) (Fig. 1E). Similarly, we observed a negative

correlation between COPD macrophage efferocytosis and high CAT scores, representative

of increased symptom severity (Fig. 1F). Correlation between bacterial phagocytosis in

COPD macrophages and both FEV1 and high CAT scores has previously been published

by our group[7]. Macrophage bacterial internalization (fig. E1A) and efferocytosis (fig. E1B)

did not correlate with study participant age. Crucially, there was a high degree of

correlation in both AM and MDM between bacterial phagocytosis and efferocytosis

within each study participant (Fig. 1G-H). Together with conservation of phenotype

between AM (Tissue) and MDM (blood) derived cells, these observations led us to

question whether a shared intrinsic defect was driving impaired phagocytosis and

efferocytosis in COPD macrophages.

COPD macrophages demonstrate a baseline defect in metabolic processing.

To explore intrinsic differences in baseline transcript abundance in AM isolated from

patients with COPD and healthy controls, we undertook Total RNA-Seq of AM isolated

from bronchoalveolar lavage, as detailed in the online supplement. Transcriptional

analysis revealed a total of 287 genes to be differentially expressed between resting

state COPD and healthy AM (Fig. 2A). In keeping with previous studies in COPD

patients, we found metabolic processes to be one of the most significantly suppressed

in COPD AM (Fig. 2B)[22,23]. As reprogramming of macrophage metabolism, particularly

mitochondrial metabolism[24], is inextricably linked to function and activation

states[25,26,27,28] , we questioned if altered metabolism in COPD macrophages results in defective cellular energetics and impaired effector function. To firstly define the energetic states of isolated AM, we undertook LC-MS analysis comparing COPD patient AM with healthy control AM. COPD AM revealed a significantly altered abundance of ATP (Fig. 2C) and concurrent reduction in energy charge status (ATP:ADP) (Fig. 2D). To establish if the altered energy state observed in COPD AM was consequent upon changes in oxidative or glycolytic metabolism, we used seahorse metabolic profiling to define basal metabolic states and metabolic reserve capacity, defined as the difference between basal and peak metabolic rates recorded after injection of metabolic stressor compounds, as outlined in the online supplement. COPD AM demonstrated equivalent extracellular acidification rates (ECAR) (fig. E2A) and reduced oxygen consumption rates (OCR) (fig. E2B) at baseline compared to healthy controls. In addition to the previously reported reduction in spare respiratory capacity[22], we observe a loss of both oxidative (Fig. 2E) and glycolytic reserve capacity (Fig. 2F) in COPD AM following exposure to metabolic stressors. Despite equivalent basal respiration and glycolytic rates (fig. E2C-D), cellular energetics were also defective in peripherally derived MDM from COPD donors, with depleted reserves in both oxidative metabolism (Fig. 2G) and glycolysis (Fig. 2H). In COPD donors, both AM and MDM reserves were unaffected by smoking status, suggesting changes in metabolism are hardwired. Moreover, changes in glycolytic enzyme abundance observed in COPD vs "healthy smoking" control AM, as detected by data-independent acquisition MS proteomic analysis, would suggest that skewing towards glycolysis is a disease specific response and not a consequence of smoking status (Fig. 2I) . While Healthy AM increased their maximal respiration rate

following co-incubation with apoptotic neutrophils (AN), COPD AM, in contrast, failed to exhibit any uplift in energetic capacity (fig. E2E and E2EF). Treatment of healthy donor AM with established M2 polarisation stimuli[28,29] did not induce a change in respiratory reserve, suggesting the spare respiratory capacity observed in healthy AM is a fundamental feature of these cells rather than a polarisation state (fig. E2G). Additionally, we did not observe a predominance of M1 or M2 markers of those detected in the proteome of COPD versus Healthy donor AM[30,31] (fig. E2H).

Defects in oxidative metabolism drive metabolic exhaustion in COPD macrophages.

With reductions in both oxidative and glycolytic reserve observed, we next questioned which metabolic processes predominate at baseline and in challenged states. Compared to healthy AM, COPD AM had a significantly reduced OCR/ECAR ratio (Fig. 3A). This preponderance for glycolysis over oxidative metabolism was again demonstrated by significantly reduced ATP-linked-OCR in COPD AM compared to healthy AM (Fig. 3B). Interestingly, while absolute ATP- linked OCR was reduced, it did represent a significantly higher percentage of maximal respiration in COPD AM during mitochondrial stress testing (Fig 3C). This suggests a lack of redundancy in mitochondrial units in COPD AM, whereby these cells are seemingly unable to recruit additional mitochondria or to further increase ATP production in existing mitochondria. Strikingly, this occurred in the presence of comparable protein abundance of the critical

ATP generating complex, Mitochondrial ATP Synthase or Complex V subunits (Fig. 3D), conserved mitochondrial to nuclear DNA ratios and comparable abundance of key mitochondrial fusion and fission proteins (Fig. 3E, fig. E3A).

To evaluate how cells differentially employed either metabolic pathway to meet increased energy demand, absolute change in ECAR was plotted against absolute change in OCR, following injection of stressor compounds. While healthy AM increased both ECAR and OCR rates, COPD AM revealed a defective induction in oxygen consumption rates (Fig 3F), a response magnified when concurrently challenged to undergo normal effector function by efferocytosing apoptotic neutrophils (Fig. 3G). Thus, COPD macrophages fail to induce oxidative metabolism with an over reliance on glycolytic energy.

To more directly identify metabolic blocks in COPD, we undertook HPLC-MS analysis of both COPD and healthy donor macrophages at rest. COPD MDM (Fig. 3H) and AM (Fig. 3I) both demonstrated a significant increase in abundance of glycolytic intermediaries compared to healthy control cells, supporting a glycolytic switch in the context of COPD (Fig. 3J). This was independent of BAL nutrient availability (fig. E3B-C), macrophage glucose uptake (fig. E3E-G) or glycogen storage (fig. E3H), suggesting differential substrate availability is not driving this phenomenon. Interestingly, BAL lactate, however, was significantly higher in COPD donors (fig. E3D). To investigate if the basal reliance on glycolysis and defective induction in oxygen consumption under conditions of activation and stress were regulated at a transcriptional level, we conducted a targeted analysis of a previously published affymetrix microarray data set from our group[7],in which AM were cultured in the presence of *S. pneumoniae*, as detailed in the online supplement. In keeping with a failure to induce oxidative

metabolism, COPD AM failed to induce any genes associated with oxidative phosphorylation in contrast to healthy control AM following exposure to *S. pneumoniae* (Fig. 3K). Conversely, upregulation of glycolytic genes in COPD AM represented 10% of the total genes upregulated in response to infection.

Loss of malic enzyme 1, a critical regulator of macrophage oxidative metabolism and redox buffering, recapitulates COPD macrophage dysfunction.

Further analysis of the metabolic signature detected by Total RNA-Sequencing of COPD versus Healthy donor AM (Fig. 2A) revealed a complete downregulation of malic enzyme 1 transcript (*ME1*) in COPD AM (Fig. 4A). This was associated with a marked reduction in ME1 protein expression within the lung macrophage compartment in patients with COPD (Fig. 4B). ME1 catalyses the reversible oxidative decarboxylation of malate to pyruvate, resulting in replenishment of TCA cycle intermediaries and the conversion of NADP+ into NADPH. As a consequence loss of ME1 has been shown to disrupt redox balance and antioxidant defence with reduced GSH:GSSG ratios[32] and induction of HO-1 in PC3 and HCT116 cell lines[33]. Thus, we sought to assess whether suppression of macrophage *ME1* recapitulates the metabolic defects observed in COPD. We used a CRISPR cas9 system to delete *ME1* from the THP-1 macrophage cell line (fig. E4A) coupled with a chemical ME1 inhibitor in healthy MDM cells. In keeping with our observed COPD phenotype, *ME1* loss resulted in a reduction in OCR:ECAR ratios (Fig. 4C) and a reduction in TCA cycle intermediaries (Fig. 4D). These metabolic adaptations were associated with a reduction in redox capacity as evidenced by a reduced GSH:GSSG ratio and high basal mROS levels (Fig. 4E-F). A

proportional increase of ^{13}C glucose incorporation into lactate in *ME1* deficient cells

(Fig. 4G), as previously reported in the HCT116 cell line[33], revealed that in the setting of

impaired oxidative phosphorylation, macrophages adapted by increasing glycolytic flux.

Importantly, this observed increase in glycolysis was, however, insufficient to confer

effective macrophage function, as evidenced by reduced efferocytosis rates in *ME1* KO

cells, mirroring the defects detected in COPD macrophages (Fig. 4H). In keeping with a

critical role for oxidative phosphorylation in macrophage efferocytosis, healthy MDM

treated with oligomycin also displayed suppressed efferocytosis (Fig. 4I). Glycolysis

only contributed to efferocytic capacity when oxidative phosphorylation was blocked

(Fig. 4I).

As ME1 loss has been associated with senescence[33] and senescence has been linked

with skewing towards glycolysis in human fibroblasts[34], we next surveyed established

markers of senescence[35], in the proteome of AM recovered from healthy non-smokers,

"healthy smokers" (defined as current smokers with normal spirometry) and patients

with COPD. There was no consistent pattern of expression to support a senescent

switch within the COPD AM accounting for the change in metabolic and effector function

(fig. E5A-F). We therefore propose that ME1 plays a key role in dictating redox buffering

capacity and metabolic flux in macrophages and that loss of ME1 skews cells towards

glycolysis and leads to impaired effector function. Metabolic and functional phenotyping

of ME1 loss recapitulated core elements of COPD macrophage dysfunction,

establishing ME1 to be an important regulator of macrophage function in both health

and disease states.

Activation of NRF2 rescues ME1 expression, reprogrammes metabolism, improving cellular energetics and redox balance and restores function in COPD Macrophages .

Previous GWAS[36], cellular[13,37,38] and murine[39] studies have identified a potential role for the NRF2 mediated anti-oxidant transcriptional response in the pathogenesis of COPD. More recently work from our group has shown that augmentation of NRF2 activity can improve bacterial phagocytic capacity in COPD macrophages[7]. Whilst the mechanisms by which NRF2 agonists recover COPD macrophage effector function remain to be fully elucidated, previous studies have suggested that NRF2 augmentation of non-opsonic bacterial phagocytosis in COPD occurs in part via upregulation of the scavenger receptor MARCO[13]. We observe loss of expression of both MARCO and the NRF2 independent Class A scavenger receptors SRA1 and SRA4 in COPD AM (fig. E6A-C). In MEFS isolated from mice lacking *Nrf2*, *Nrf2* has also been shown to modulate mitochondrial respiration and ATP levels [40]. Moreover, studies in human lymphoid and cancer cell lines have identified ME1 to be a target gene of NRF2[41,42]. Given the inherent shared defect we observed in both efferocytosis and opsonic phagocytosis, we therefore questioned whether a specific NRF2 agonist KI-696[7,43], could in part mediate its effect by overcoming the intrinsic metabolic defects observed in COPD AM and MDM.

Activation of NRF2 via KI-696 significantly increased *ME1* expression in COPD macrophages, as anticipated (Fig. 5A). In keeping with the established role for ME1 in generating NADPH, we also observed an improvement in GSH:GSSG ratios and an increase in total glutathione availability in COPD macrophages following treatment with

KI-696 (Fig. 5B-C). To more directly measure the effects of NRF2 agonists on the

metabolic capacity of COPD AM, we undertook LC-MS analysis of AM from COPD

patients treated with KI-696 and compared these to untreated COPD and healthy

control AM. KI-696 mediated NRF2 activation did not significantly alter glycolytic

metabolite abundance (Fig. 5D). However, it did significantly increase the abundance of

all TCA cycle intermediaries relative to baseline abundance in untreated COPD AM

(Fig. 5E) and partially restored cellular energetics (Fig. 5F).

To address the processes underlying this metabolic rescue, RNAseq analysis was

performed on AM from healthy donors and COPD patients at baseline and following

treatment with KI-696. Correlation analysis across the 30,000 gene set revealed that

COPD AM were more highly correlated with healthy AM following treatment with KI-696

(Fig. 6A-D). "Regulation of metabolic processes" was the most differentially upregulated

biological process in COPD AM following NRF2 activation (Fig. 6E). Amongst *ME1*,

other metabolic genes of interest altered by NRF2 activation of COPD AM, included

G6PC3, MAPK14, TLK1 and OARD1 (Fig 6C-D). Finally, we questioned if the NRF2

mediated restoration of redox balance and correction of disturbances in oxidative

metabolism and cellular energetics could rescue COPD macrophage efferocytosis.

COPD MDM and AM both improved efferocytic capacity in the continued presence of

the NRF2 agonist KI-696 (Fig 6F-G and fig. E6D). Failure of KI-696 to recover

efferocytosis in *ME1* KO cells, would suggest that augmentation of ME1 expression is

required for NRF2 mediated enhancement of efferocytosis (fig. E6E). Figure 6H

summarizes the functional outcomes associated with impaired metabolic plasticity in

COPD macrophages and therapeutic rescue with NRF2 activation.

Discussion

COPD is characterized by persistent inflammation of the airways, destruction of lung tissue and mucus hypersecretion resulting in airflow limitation and impaired gas exchange. Pathogen colonization and recurrent infective exacerbations are the largest contributor to morbidity and mortality within the disease[3]. Failure of COPD macrophages to adequately phagocytose and kill bacteria and to instigate inflammation resolution via efferocytosis, places macrophage dysfunction at the centre of both disease pathology and progression in COPD[5,12,44]. Study of alveolar macrophages, directly influenced by the lung microenvironment and peripherally derived monocyte-derived macrophages, has enabled us to define an intrinsic metabolic defect in COPD macrophages which drives this functional impairment. Extending from previous descriptions of diminished baseline respiratory reserve capacity in COPD AM[22], we describe a more global defect in COPD macrophage bioenergetics when these cells are engaged to undertake the highly energy requiring process of efferocytosis. Moreover, we provide evidence that defective metabolism is not an exclusive consequence of an inflamed pulmonary niche by also characterising this metabolic exhaustion, although to a lesser degree, in peripherally circulating MDM. Within the limitations of the small number of healthy smoker controls included in this study, defective metabolism would also appear to be independent of current smoking status, with evidence of alterations in glycolytic enzyme abundance specific to disease state. This leads us to postulate that there is both central (bone marrow) reprogramming of newly formed monocytes which contribute to replenishment of the alveolar macrophage compartment in the diseased lung and

peripheral (lung tissue) reprogramming of the alveolar macrophage compartment following exposure to the local inflammatory milieu and metabolic intermediaries. This concept is supported by emerging evidence that reprogramming of myelopoiesis has consequence for myeloid cell tissue effector functions in acute[45] and chronic inflammatory disease states[6,24], with overlapping transcriptional signatures previously reported in COPD MDM and AM populations[46] and evidence of changes in DNA accessibility and methylation marks in the AM compartment during trained immune responses[47,48].Metabolic plasticity is a crucial feature of macrophage adaptability, with the capacity to generate ATP via multiple metabolic pathways, namely glycolysis, oxidative phosphorylation and fatty acid oxidation[25,28]. Recent evidence has demonstrated that the dichotomy of glycolysis supporting acute inflammatory responses and oxidative metabolism fuelling sustained energy production is as an over simplification of macrophage bioenergetics, with significant cross talk required between these metabolic pathways[49,50,51]. Importantly, we describe a refractory metabolism in COPD macrophages with both a significant depletion in glycolytic and mitochondrial respiration derived energy reserves and an over reliance on glycolysis as a source for ATP. Further work will be required to understand how these intrinsic metabolic adaptions influence and are themselves influenced by changes in the wider pulmonary niche as exemplified by elevated BAL lactate levels in COPD donors. This vulnerability of COPD macrophages to defects in reserve energy capacity has consequence for key effector functions, with glycolysis only partially supporting healthy macrophage efferocytosis in the absence of oxidative phosphorylation.

With high oxidative stress, mitochondrial dysfunction and suppressed oxidative phosphorylation features of COPD [14,23,52,53,54], we were interested to note the basal suppression of transcript for the enzyme, malic enzyme 1 (ME1), in COPD macrophages. ME1 is the rate regulating enzyme for the cytosolic malate-pyruvate shunt. In catalysing malate conversion to pyruvate, it generates NADPH, augmenting the replenishment of reduced glutathione for redox power[32] and in turn shuttling pyruvate into the TCA cycle[55]. Replicating ME1 loss in vitro reveals its critical role in macrophage redox balance, with resulting changes in basal mROS levels, but also highlights that loss of ME1 skews macrophage metabolism away from oxidative metabolism, with consequence for effector function such as efferocytosis. The specific mechanisms by which ME1 loss drives increased glycolytic flux remain to be fully explored, and may relate not only to redox capacity but also a need to replenish intracellular pyruvate levels. To date, there is no evidence linking ME1 activity directly to macrophage polarisation states. Specifically, a malic enzyme signature was not detected in the seminal paper on macrophage phenotype metabolism by Jha et al[28]. The specific mechanisms driving the depletion of ME1 in COPD are a subject for future work. Of note however, we observe changes in ME1 expression to occur at both a protein and transcript level. Coupled with evidence of altered activity of the ME1 transcriptional regulator NRF2, in the small airways of patients with COPD[56], global changes in DNA methylation states, and correlation between HDAC2 and NRF2 expression in COPD MDM[57], this supports the concept of intrinsic rewiring of macrophage responses. We speculate that epigenetic changes within the bone-marrow compartment would enable this reprogramming of the mononuclear phagocyte system

with further modification by local cues within the airways of patients with COPD. We propose that it is the interplay between these central and peripheral epigenetic programs that regulates ME1 expression, with consequent changes in AM and MDM core effector functions.

Whilst ME1 was the only gene directly regulated by NRF2 which showed differential regulation at baseline in RNA-seq data sets comparing healthy control AM with COPD AM, previous work by our group has demonstrated a relative increase in protein expression of the NRF2 targets GLCL, NQO1 and HO-1 following NRF2 activation of COPD macrophages[7]. It is likely, therefore, that ME1 is one of a number of factors contributing to the metabolic defects observed in COPD and responsive to NRF2 augmentation. This is further supported by our observation that other metabolic genes including G6PC3, MAPK14,TLK1 and OARD1 are altered by activation of NRF2 activation in COPD AM, and the incomplete rescue of COPD macrophage effector function by KI-696. Understanding how regulators of transcriptional programmes and metabolic plasticity in COPD macrophages interact with processes that are responsive to NRF2 augmentation to rescue effector function will be essential for the development of new therapeutic strategies. Equally, study of patients with early disease and smokers who have airway inflammation but are yet to develop airflow obstruction, will also be of importance in defining the temporal relationship between defective macrophage metabolism and disease progression.

Acknowledgements:

References:

1.	Willemse B, Hacken Ten N. Effect of 1-year smoking cessation on airway inflammation in COPD and asymptomatic smokers. *European ….* 2005.

2.	Hogg JC, Chu F, Utokaparch S, et al. The Nature of Small-Airway Obstruction in Chronic Obstructive Pulmonary Disease. *The New England journal of medicine*. 2004;350(26):2645-2653. doi:10.1056/NEJMoa032158.

3.	Patel IS, Seemungal TAR, Wilks M, Lloyd-Owen SJ, Donaldson GC, Wedzicha JA. Relationship between bacterial colonisation and the frequency, character, and severity of COPD exacerbations. *Thorax*. 2002;57(9):759-764. doi:10.1136/thorax.57.9.759.

4.	Oltmanns U, Sukkar MB, Xie S, John M, Chung KF. Induction of human airway smooth muscle apoptosis by neutrophils and neutrophil elastase. *Am J Respir Cell Mol Biol*. 2005;32(4):334-341. doi:10.1165/rcmb.2004-0321OC.

5.	Berenson CS, Garlipp MA, Grove LJ, Maloney J, Sethi S. Impaired phagocytosis of nontypeable Haemophilus influenzae by human alveolar macrophages in chronic obstructive pulmonary disease. *J Infect Dis*. 2006;194(10):1375-1384. doi:10.1086/508428.

6.	Taylor AE, Finney-Hayward TK, Quint JK, et al. Defective macrophage phagocytosis of bacteria in COPD. *European Respiratory Journal*. 2010;35(5):1039-1047. doi:10.1183/09031936.00036709.

7.   Bewley MA, Budd RC, Ryan E, et al. Opsonic Phagocytosis in Chronic

        Obstructive Pulmonary Disease Is Enhanced by Nrf2 Agonists. *Am J Respir*

        Crit Care Med. 2018;198(6):739-750. doi:10.1164/rccm.201705-0903OC.

8.   Hodge S, Hodge G, Ahern J, Jersmann H, Holmes M, Reynolds PN. Smoking

        Alters Alveolar Macrophage Recognition and Phagocytic Ability. *Am J Respir*

        Cell Mol Biol. 2007;37(6):748-755. doi:10.1165/rcmb.2007-0025OC.

9.   Russell REK, Culpitt SV, DeMatos C, et al. Release and activity of matrix

        metalloproteinase-9 and tissue inhibitor of metalloproteinase-1 by alveolar

        macrophages from patients with chronic obstructive pulmonary disease. *Am J*

        Respir Cell Mol Biol. 2002;26(5):602-609. doi:10.1165/ajrcmb.26.5.4685.

10.   Molet S, Belleguic C, Lena H, et al. Increase in macrophage elastase (MMP-

        12) in lungs from patients with chronic obstructive pulmonary disease. *Inflamm*

        Res. 2005;54(1):31-36. doi:10.1007/s00011-004-1319-4.

11.   Hiemstra PS. Altered macrophage function in chronic obstructive pulmonary

        disease. *Annals ATS*. 2013;10 Suppl(Supplement):S180-S185.

        doi:10.1513/AnnalsATS.201305-123AW.

12.   Bewley MA, Preston JA, Mohasin M, et al. Impaired Mitochondrial Microbicidal

        Responses in Chronic Obstructive Pulmonary Disease Macrophages. *Am J*

        Respir Crit Care Med. 2017;196(7):845-855. doi:10.1164/rccm.201608-

        1714OC.

13. Harvey CJ, Thimmulappa RK, Sethi S, et al. Targeting Nrf2 Signaling Improves Bacterial Clearance by Alveolar Macrophages in Patients with COPD and in a Mouse Model. *Science Translational Medicine*. 2011;3(78):78ra32-78ra32. doi:10.1126/scitranslmed.3002042.

14. Cloonan SM, Glass K, Laucho-Contreras ME, et al. Mitochondrial iron chelation ameliorates cigarette smoke-induced bronchitis and emphysema in mice. *Nature Medicine 2016 22:9*. 2016;22(2):163-174. doi:10.1038/nm.4021.

15. Ryan EM, Coelho P, Cole J, et al. T1 Defective metabolism drives macrophage dysfunction in COPD. *Thorax*. 2021;76(Suppl 1):A1.

16. Ryan EM, Budd R, Bewley MA, COPD PCSI, 2018. Impaired Bioenergetic Profile of COPD Macrophages. *Atsjournalsorg.*

17. Ryan EM, Budd R, Bewley MA, et al. S115 Mechanisms to reverse impaired macrophage efferocytosis in copd. *Thorax*. 2017;72(Suppl 3):A70-A70. doi:10.1136/thoraxjnl-2017-210983.121.

18. Cacciottolo TM, Perikari A, van der Klaauw A, et al. Scientific Business Abstracts of the 113th Annual Meeting of the Association of Physicians of Great Britain and Ireland. *QJM*. 2019;112(9):724-729. doi:10.1093/qjmed/hcz175.

19. Gordon SB, Irving GR, Lawson RA, Lee ME, Read RC. Intracellular trafficking and killing of Streptococcus pneumoniae by human alveolar macrophages are influenced by opsonins. *Infect Immun*. 2000;68(4):2286-2293.

20.   Bewley MA, Belchamber KBR, Chana KK, et al. Differential Effects of p38,

MAPK, PI3K or Rho Kinase Inhibitors on Bacterial Phagocytosis and

Efferocytosis by Macrophages in COPD. Maus UA, ed. *PLoS ONE*.

2016;11(9):e0163139. doi:10.1371/journal.pone.0163139.

21.   Hodge S, Matthews G, Mukaro V, et al. Cigarette smoke-induced changes to

alveolar macrophage phenotype and function are improved by treatment with

procysteine. *Am J Respir Cell Mol Biol*. 2011;44(5):673-681.

doi:10.1165/rcmb.2009-0459OC.

22.   O'Beirne SL, Kikkers SA, Oromendia C, et al. Alveolar Macrophage

Immunometabolism and Lung Function Impairment in Smoking and Chronic

Obstructive Pulmonary Disease. *Am J Respir Crit Care Med*. 2020;201(6):735-

739. doi:10.1164/rccm.201908-1683LE.

23.   Kim WJ, Lim JH, Lee JS, Lee S-D, Kim JH, Oh Y-M. Comprehensive Analysis

of Transcriptome Sequencing Data in the Lung Tissues of COPD Subjects. *Int

J Genomics*. 2015;2015:206937-206939. doi:10.1155/2015/206937.

24.   Belchamber KBR, Singh R, Batista CM, et al. Defective bacterial phagocytosis

is associated with dysfunctional mitochondria in COPD macrophages. *Eur

Respir J*. 2019;54(4). doi:10.1183/13993003.02244-2018.

25.   Rodriguez-Prados J-C, Traves PG, Cuenca J, et al. Substrate fate in activated

macrophages: a comparison between innate, classic, and alternative

activation. *J Immunol*. 2010;185(1):605-614. doi:10.4049/jimmunol.0901698.

26.   Freemerman AJ, Johnson AR, Sacks GN, et al. Metabolic reprogramming of macrophages: glucose transporter 1 (GLUT1)-mediated glucose metabolism drives a proinflammatory phenotype. *J Biol Chem*. 2014;289(11):7884-7896. doi:10.1074/jbc.M113.522037.

27.   Vats D, Mukundan L, Odegaard JI, et al. Oxidative metabolism and PGC-1β attenuate macrophage-mediated inflammation. *Cell Metabolism*. 2006;4(1):13-24. doi:10.1016/j.cmet.2006.05.011.

28.   Jha AK, Huang SC-C, Sergushichev A, et al. Network integration of parallel metabolic and transcriptional data reveals metabolic modules that regulate macrophage polarization. *Immunity*. 2015;42(3):419-430. doi:10.1016/j.immuni.2015.02.005.

29.   Zhang S, Weinberg S, DeBerge M, et al. Efferocytosis Fuels Requirements of Fatty Acid Oxidation and the Electron Transport Chain to Polarize Macrophages for Tissue Repair. *Cell Metabolism*. 2019;29(2):443-456.e445. doi:10.1016/j.cmet.2018.12.004.

30.   Becker L, Liu N-C, Averill MM, et al. Unique proteomic signatures distinguish macrophages and dendritic cells. *PLoS ONE*. 2012;7(3):e33297. doi:10.1371/journal.pone.0033297.

31.   Court M, Petre G, Atifi ME, Millet A. Proteomic Signature Reveals Modulation of Human Macrophage Polarization and Functions Under Differing

Environmental Oxygen Conditions. *Mol Cell Proteomics*. 2017;16(12):2153-2168. doi:10.1074/mcp.RA117.000082.

32.   Zheng F-J, Ye H-B, Wu M-S, Lian Y-F, Qian C-N, Zeng Y-X. Repressing malic enzyme 1 redirects glucose metabolism, unbalances the redox state, and attenuates migratory and invasive abilities in nasopharyngeal carcinoma cell lines. *Chin J Cancer*. 2012;31(11):519-531. doi:10.5732/cjc.012.10088.

33.   Murai S, Ando A, Ebara S, Hirayama M, Satomi Y, Hara T. Inhibition of malic enzyme 1 disrupts cellular metabolism and leads to vulnerability in cancer cells in glucose-restricted conditions. *Oncogenesis 2017 6:5*. 2017;6(5):e329-e329. doi:10.1038/oncsis.2017.34.

34.   Coppé J-P, Desprez P-Y, Krtolica A, Campisi J. The senescence-associated secretory phenotype: the dark side of tumor suppression. *Annu Rev Pathol*. 2010;5:99-118. doi:10.1146/annurev-pathol-121808-102144.

35.   Hassibi S, Baker J, Barnes P, Donnelly L. COPD Monocyte-derived macrophages display hallmarks of senescence. 2022.

36.   Korytina GF, Akhmadishina LZ, Aznabaeva YG, et al. Associations of the NRF2/KEAP1 pathway and antioxidant defense gene polymorphisms with chronic obstructive pulmonary disease. *Gene*. 2019;692:102-112. doi:10.1016/j.gene.2018.12.061.

37.   Suzuki M, Betsuyaku T, Ito Y, et al. Down-Regulated NF-E2–Related Factor 2 in Pulmonary Macrophages of Aged Smokers and Patients with Chronic

Obstructive Pulmonary Disease. *Am J Respir Cell Mol Biol*. 2008;39(6):673-682. doi:10.1165/rcmb.2007-0424OC.

38.   Goven D, Boutten A, Leçon-Malas V, et al. Altered Nrf2/Keap1-Bach1 equilibrium in pulmonary emphysema. *Thorax*. 2008;63(10):916-924. doi:10.1136/thx.2007.091181.

39.   Rangasamy T, Cho CY, Thimmulappa RK, et al. Genetic ablation of Nrf2 enhances susceptibility to cigarette smoke-induced emphysema in mice. *J Clin Invest*. 2004;114(9):1248-1259. doi:10.1172/JCI21146.

40.   Holmström KM, Baird L, Zhang Y, et al. Nrf2 impacts cellular bioenergetics by controlling substrate availability for mitochondrial respiration. *Biol Open*. 2013;2(8):761-770. doi:10.1242/bio.20134853.

41.   Thimmulappa RK, Mai KH, Srisuma S, Kensler TW, Yamamoto M, Biswal S. Identification of Nrf2-regulated genes induced by the chemopreventive agent sulforaphane by oligonucleotide microarray. *Cancer Res*. 2002;62(18):5196-5203.

42.   Chorley BN, Campbell MR, Wang X, et al. Identification of novel NRF2-regulated genes by ChIP-Seq: influence on retinoid X receptor alpha. *Nucleic Acids Res*. 2012;40(15):7416-7429. doi:10.1093/nar/gks409.

43.   Davies TG, Wixted WE, Coyle JE, et al. Monoacidic Inhibitors of the Kelch-like ECH-Associated Protein 1: Nuclear Factor Erythroid 2-Related Factor 2 (KEAP1:NRF2) Protein-Protein Interaction with High Cell Potency Identified by

Fragment-Based Discovery. *J Med Chem*. 2016;59(8):3991-4006. doi:10.1021/acs.jmedchem.6b00228.

44.   Hodge S, Hodge G, Scicchitano R, Reynolds PN, Holmes M. Alveolar macrophages from subjects with chronic obstructive pulmonary disease are deficient in their ability to phagocytose apoptotic airway epithelial cells. *Immunol Cell Biol*. 2003;81(4):289-296. doi:10.1046/j.1440-1711.2003.t01-1-01170.x.

45.   Mirchandani AS, Jenkins SJ, Bain CC, et al. Hypoxia shapes the immune landscape in lung injury and promotes the persistence of inflammation. *Nat Immunol*. 2022;23(6):927-939. doi:10.1038/s41590-022-01216-z.

46.   Poliska S, Csanky E, Szanto A, et al. Chronic obstructive pulmonary disease-specific gene expression signatures of alveolar macrophages as well as peripheral blood monocytes overlap and correlate with lung function. *Respiration*. 2011;81(6):499-510. doi:10.1159/000324297.

47.   Schultze JL, Mass E, Schlitzer A. Emerging Principles in Myelopoiesis at Homeostasis and during Infection and Inflammation. *Immunity*. 2019;50(2):288-301. doi:10.1016/j.immuni.2019.01.019.

48.   Yao Y, Jeyanathan M, Haddadi S, et al. Induction of Autonomous Memory Alveolar Macrophages Requires T Cell Help and Is Critical to Trained Immunity. *Cell*. 2018;175(6):1634–1650.e17. doi:10.1016/j.cell.2018.09.042.

49.   Namgaladze D, Brüne B. Fatty acid oxidation is dispensable for human macrophage IL-4-induced polarization. *Biochimica et Biophysica Acta (BBA) - Molecular and Cell Biology of Lipids*. 2014;1841(9):1329-1335. doi:10.1016/j.bbalip.2014.06.007.

50.   Moon J-S, Nakahira K, Chung K-P, et al. NOX4-dependent fatty acid oxidation promotes NLRP3 inflammasome activation in macrophages. *Nature Medicine 2016 22:9*. 2016;22(9):1002-1012. doi:10.1038/nm.4153.

51.   Van den Bossche J, Baardman J, Otto NA, et al. Mitochondrial Dysfunction Prevents Repolarization of Inflammatory Macrophages. *Cell reports*. 2016;17(3):684-696. doi:10.1016/j.celrep.2016.09.008.

52.   Wiegman CH, Michaeloudes C, Haji G, et al. Oxidative stress-induced mitochondrial dysfunction drives inflammation and airway smooth muscle remodeling in patients with chronic obstructive pulmonary disease. *J Allergy Clin Immunol*. 2015;136(3):769-780. doi:10.1016/j.jaci.2015.01.046.

53.   Ahmad T, Sundar IK, Lerner CA, et al. Impaired mitophagy leads to cigarette smoke stress-induced cellular senescence: implications for chronic obstructive pulmonary disease. *FASEB J*. 2015;29(7):2912-2929. doi:10.1096/fj.14-268276.

54.   Gleeson LE, O'Leary SM, Ryan D, McLaughlin AM, Sheedy FJ, Keane J. Cigarette Smoking Impairs the Bioenergetic Immune Response to

Mycobacterium tuberculosis Infection. *Am J Respir Cell Mol Biol*.
2018;59(5):572-579. doi:10.1165/rcmb.2018-0162OC.

55.   Deberardinis RJ, Mancuso A, Thompsom CB. Beyond aerobic glycolysis:
        Transformed cells can engage in glutamine metabolism that exceeds the
        requirement for protein and nucleotide synthesis. *PNAS*.
        doi:10.1073/pnas.0709747104.

56.   Vucic EA, Chari R, Thu KL, et al. DNA methylation is globally disrupted and
        associated with expression changes in chronic obstructive pulmonary disease
        small airways. *Am J Respir Cell Mol Biol*. 2014;50(5):912-922.
        doi:10.1165/rcmb.2013-0304OC.

57.   Mercado N, Thimmulappa R, Thomas CMR, et al. Decreased histone
        deacetylase 2 impairs Nrf2 activation by oxidative stress. *Biochem Biophys
        Res Commun*. 2011;406(2):292-298. doi:10.1016/j.bbrc.2011.02.035.

Figure legends :

Figure 1. Intrinsic defects in COPD alveolar and peripheral blood monocyte-derived macrophages. (A-B) Alveolar (AM) and Monocyte-Derived Macrophages (MDM) from healthy controls (squares) and COPD donors (circles) were challenged with opsonised serotype 14 *S. pneumoniae* for 4 hours and numbers of viable bacteria measured or **(C-D)** co-incubated with PKH26 labelled 20h apoptotic neutrophils and efferocytosis rates measured by flow cytometry. (A, HC n=6, COPD n= 8, B, HC/COPD n=8 , C, HC n=8, COPD n=11; D, HC/COPD n=10). (**E-F**) COPD AM and MDM efferocytosis were correlated with FEV1% (E, n=14) and symptoms of disease severity, as measured by the CAT score (F, n=24). (**G-H**) Efferocytosis of PKH26 labelled apoptotic neutrophils was correlated with phagocytosis of *S. pneumoniae* S14 in both Alveolar (G, n=13) and Monocyte- Derived Macrophages (H, n= 24) from COPD and healthy donors. Open squares and circles represent current smokers. Data represent individual values with mean ± SEM. P values calculated by unpaired t-test, *P ≤0.05, ***P≤0.001, ****P≤0.0001. Pearson's correlation coefficient (r) as shown.

Figure 2. Loss of energy reserves in COPD macrophages. (**A**-**B**) AM were isolated from COPD and healthy donors via bronchoalveolar lavage, cultured for 16 hours prior to collecting RNA for Total RNA-seq, n=3. **(A)** Volcano plots displaying the $\log_2$ fold change (FC) between COPD and healthy donors. Red dots (n=287) represent genes which are significantly altered. Orange dots represent genes which are altered but do not meet significance. **(B)** Top four Gene Ontology (GO) processes upregulated in healthy AM, at baseline, compared to COPD AM. (**C**-**D**) HPLC-MS analysis was carried out to determine the levels of ATP, ADP and AMP in resting state healthy donor (squares) and COPD

(circles) AM and energy charge ([ATP+1/2ADP]/ (ATP+ADP+AMP]) was calculated (n=5/6).

(**E-H**) Seahorse mitochondrial (**E, G**) and glycolytic (**F, H**) stress testing in COPD AM and

MDM. (E, HC n=9, COPD n=12, F, HC n=6 COPD n=10, G, n=7, H, n=5). Open squares

and circles indicate current smokers. COPD Smoker vs Ex-Smoker, E, p value= 0.103, F, p

value= 0.158, G, p value = 0.17. (**I**) Glycolytic enzyme abundance in COPD (n=7) versus

"Healthy Smoker" (HS) AM (n=5) as determined by data-independent acquisition MS

proteomic analysis. Data represents individual values ± SEM. (A-B) Significance

determined at FC >$\log_2$1.5 and p value ≤ 0.05. P values calculated via (C,I) 2-way ANOVA,

(E,F,G) unpaired t-test, (D+H) Mann Whitney U Test. *P ≤0.05, **P≤0.01, ****P≤0.0001.

ECAR= Extracellular acidification rate, OCR= oxygen consumption rate. HPLC-MS= High

performance liquid chromatography mass spectrometry. FC =Fold change.

Figure 3. COPD macrophages display a preponderance for glycolytic metabolism.

(**A**) Calculated OCR/ECAR ratio in healthy (squares) and COPD (circles) AM (**B**) OCR

consumption linked to ATP generation in healthy and COPD AM as calculated by the

reduction in OCR following oligomycin treatment. (**C**) ATP-linked-OCR as a percentage of

maximal OCR in healthy and COPD AM. HC n=9, COPD N=12. (**D)** Relative protein

abundance of the 11 detected subunits of Mitochondrial ATP Synthase/ Complex V, as

measured by data-independent acquisition MS proteomic analysis. COPD AM n= 7,

Healthy Non smoker (HNS) and Healthy Smoker (HS) n= 5. (**E**) AM Mitochondrial DNA to

Nuclear DNA ratios, as measured by Real-Time quantitative PCR. Healthy donor n= 6,

COPD donor n= 5. (**F-G**) Absolute change in ECAR was plotted against absolute change in

OCR following injection of mitochondrial stressor compounds in resting macrophages (F,

n=21) and after cells were co-incubated with 20h apoptotic neutrophils for 90 min (G,

n=14). (**H- I**) Glycolytic metabolite abundance determined by HPLC-MS in resting state

MDM (H, n=4) COPD AM (I, HC n= 6, COPD n=8), plotted as relative to healthy control. **(J)**

Schematic of glycolytic intermediaries increased throughout the glycolytic pathway in

COPD macrophages. (**K**) The transcriptional response in COPD and healthy control AM

following co-incubation with opsonised D39 *Streptococcus pneumoniae*, n=3. Data

represents individual values and mean ± SEM. P values calculated by (A-C) unpaired t-test,

(E) Mann Whitney U Test, (D,H,I) via 2-way ANOVA. *P≤0.05, **P≤0.01, ns= not significant,

FC= Fold Change.

Figure 4. Malic enzyme 1 (ME1) plays a critical role in macrophage metabolism

and efferocytosis. (A) Transcriptomic analysis of baseline *ME1* expression in healthy

control and COPD AM normalised to TPM (transcripts per kilobase million), n=3 (**B**)

ME1 expression in healthy and COPD patient lung sections prepared from paraffin-

embeded blocks, images taken at x20 magnification (**C**) Healthy MDM were treated x16

hours with a chemical ME1 inhibitor or DMSO control before measuring the basal

OCR:ECAR ratio on a Seahorse platform, n=7. (**D**) HPLC-MS analysis of TCA cycle

metabolite abundance in THP-1 empty vector control (EV) and *ME1* knockout (*ME1* KO)

cells, normalised to protein content, n=5. **(E)** GSH:GSSG ratio calculated in THP-1 EV

and *ME1* KO cells, n=9. **(F)** Healthy MDM were treated x16 hours with a chemical ME1

inhibitor or DMSO control. Mean fluorescence intensity of MitoSox Red was then

measured from >180 cells per condition for n= 3 donors. **(G)** U-^{13}C glucose

incorporation into lactate in THP-1 EV and *ME1* KO following 6h of culture in U-^{13}C

glucose containing media, n=6. **(H-I)** THP-1 EV and *ME1* knockout cells (H) and healthy

MDM pretreated with Oligomycin 2μM, 2DG 50mM or Oligomycin and 2DG combined

for 1hr (I) prior to co-incubation with PKH26 labelled 20h apoptotic neutrophils for 90

minutes and efferocytosis rate determined by flow cytometry, (H) n=8 (I) n= 8,8,7 and 4

respectively. Data represents individual values and mean ± SEM. P values calculated

via (A) adjusted t-test values from Total RNA-seq analysis as outlined in online

supplement, (C,E,G,H) paired t-test, (D,I) 2-way ANOVA with Dunnett's multiple

comparisons, (F) Wilcoxon matched paired signs rank test . *P≤0.05, **P≤0.01,

****P≤0.0001, ns= not significant. HPLC-MS = High performance liquid chromatography

mass spectrometry.

Figure 5. Cellular energetics and redox status are improved in COPD AM

following activation of ME1 via the NRF2 agonist KI-696. (**A**) Real-time PCR

quantification of *ME1* expression relative to β-actin in COPD AM following culture in the

absence or presence of KI-696, n=6. **(B-C)** Treatment with Ki-696 alters redox

protection in COPD AM as measured by (B) GSH:GSSG ratios and (C) absolute total

glutathione abundance (GSH and GSSG), HC n= 4, COPD n=6. (**D-E**) LC-MS analysis

of healthy and COPD AM (+/- KI-696). Metabolite abundance is plotted as relative to

untreated COPD AM (fold change) n= 7. **(F)** Energy status expressed as an ATP to ADP

ratio was calculated, n=5 . Data represents individual values and mean ± SEM. P values

calculated via (A) paired t-test, (B,C,F) Kruskal Wallis with Dunn's multiple comparison

tests and (D-E) 2-way ANOVA. *P≤0.05, **P≤0.01, ***P≤0.001.

Figure 6. Activation of NRF2 with KI-696 reprogrammes alveolar macrophages in

COPD with consequences for effector function. (**A**-**E**) Healthy and COPD AM were

cultured for 16h (+/- KI-696) prior to collection of RNA for Total RNA-seq, n=3. **(A-B)**

Correlation analysis between healthy and COPD AM pre and post treatment with KI-

696. Red dots represent significantly differentially expressed genes between COPD and Healthy AM at baseline, which are seen to move towards the trendline in (B). **(C-D)** Heatmap of normalized Z-scores showing genes which were initially comparatively downregulated (C) or upregulated (D) in COPD vs healthy AM, which were transcriptionally reprogrammed by treatment with KI-696, in the direction of healthy AM. (**E**)The lead Gene Ontology (GO) terms upregulated in COPD AM following treatment with KI-696. **(F**-**G**) COPD AM (F, HC n=2, COPD n=6) and MDM (G, HC n=5, COPD n=6) were pre-treated for 16h with the NRF2 activator KI-696, prior to co-incubation with PKH26 labelled 20h apoptotic neutrophils and measurement of efferocytosis rates by flow cytometry.(H) Summary diagram of metabolic changes in COPD macrophages and the role of NRF2 augmentation. Data represents individual values and mean ± SEM. (A-B) Scatter plots were generated by plotting the average Log_2 Tags Per Million (TPM) scores for healthy AM vs the average Log2 TPM scores for COPD AM +/- KI-696. R^2 squared values were calculated from the slope of the correlation trendline. DE genes= FC > $log_2$1.5 and P value≤0.05. (F-G) P values calculated via (F) paired t-test (G) COPD donors paired t- test and healthy donors Wilcoxon matched paired signs rank test. **P≤0.01, ***P≤0.001.

	Healthy Non smokers	"Healthy Smokers"	Subjects with COPD
No of Subjects	24	9	52
Age (yr)	54 (31-70)	53 (36-68)	61 (39-77)
Sex female/male	12/12	2/7	29/23
FEV1 (L)	3.1 ± 0.7	3.5 ± 0.3	1.7 ± 0.5
FEV1 (% predicted)	105 ± 12.9	98 ± 4.1	64 ± 10.11
Gold Stage	N/A	N/A	14 Stage 1 26 Stage 2 11 Stage 3 1 Stage 4
Exacerbation per year 0/ >1/>2 / ≥3	N/A	N/A	14/10/20/8
Smoking status Current/Ex/Never	0/0/24	9/0/0	23/29/0
Pack years	n/a	30 ± 10	37 ± 14
CAT score (Max 40)	N/A	N/A	16 ± 8
Inhaled Medication: ICS+LABA / LAMA / SABA	N/A	N/A	25/27/34

Table 1: Demographics of study participants. Healthy Non-smokers = Lifelong non-smokers with normal spirometry. Healthy smokers = current smokers with normal spirometry. COPD donors = current or ex-smokers with an FEV1/FVC ratio of <0.70.
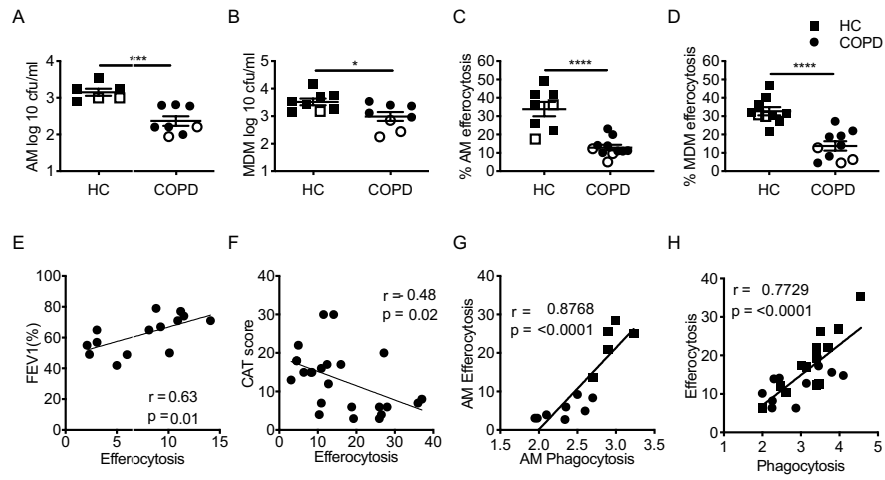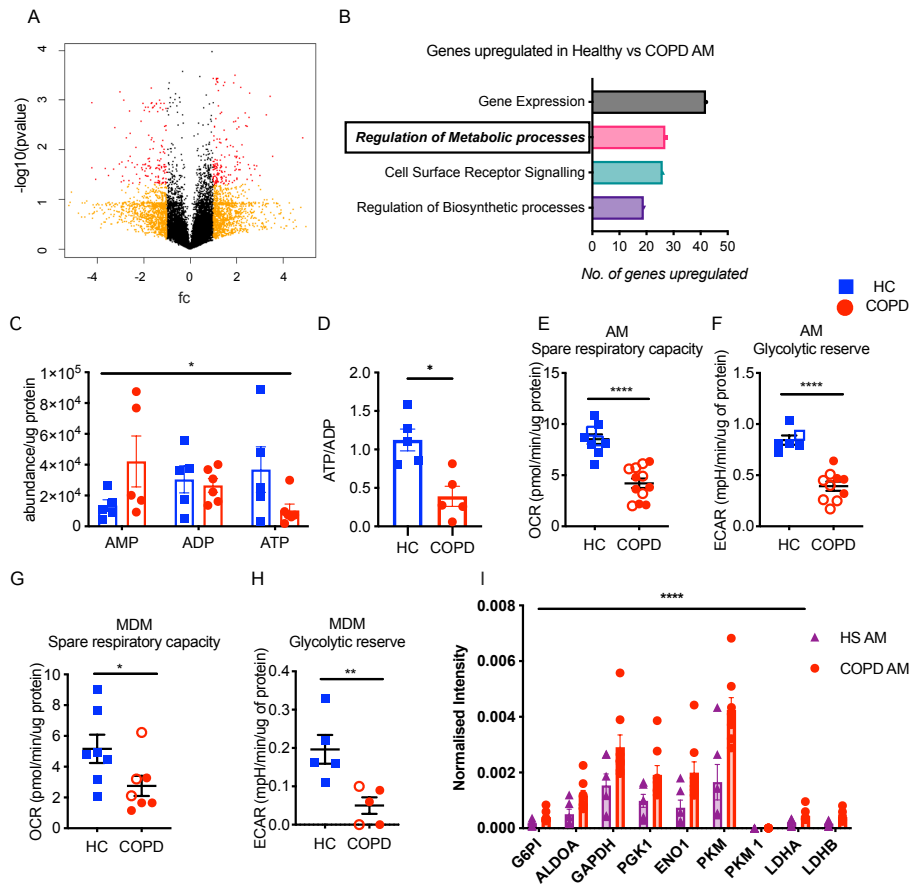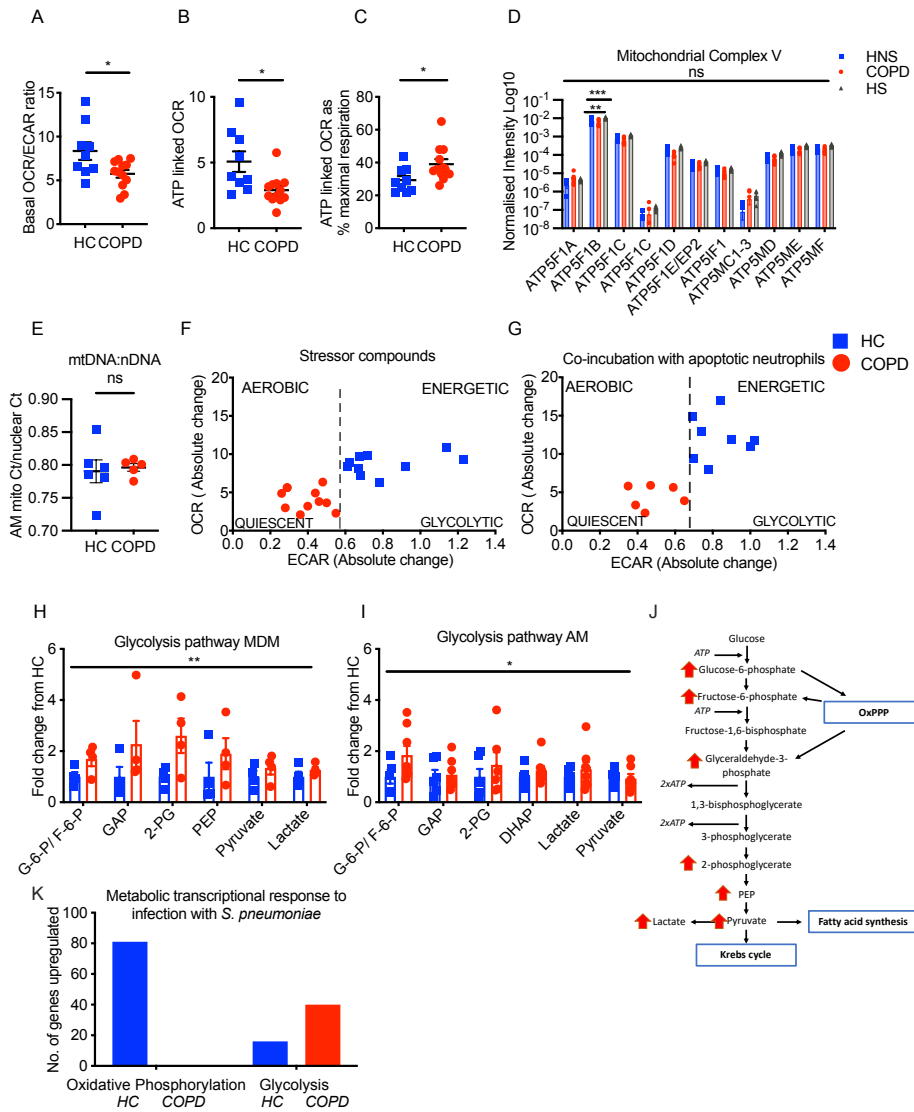
Figure 1:
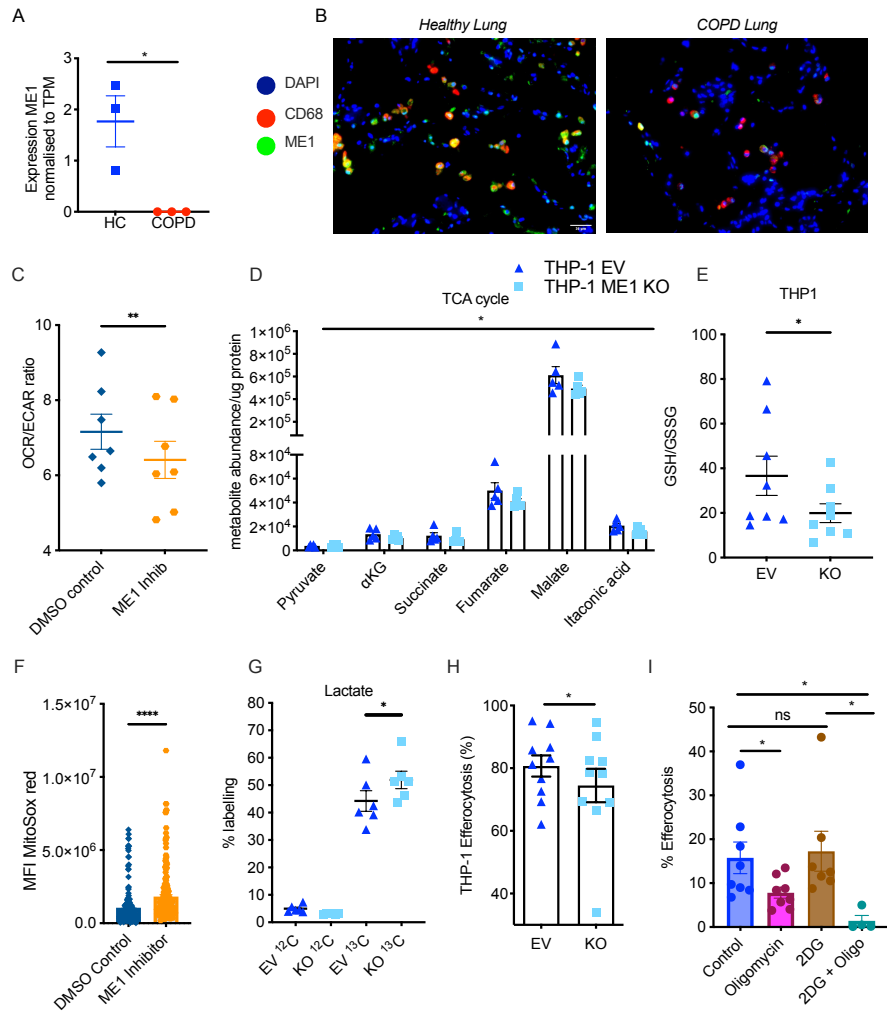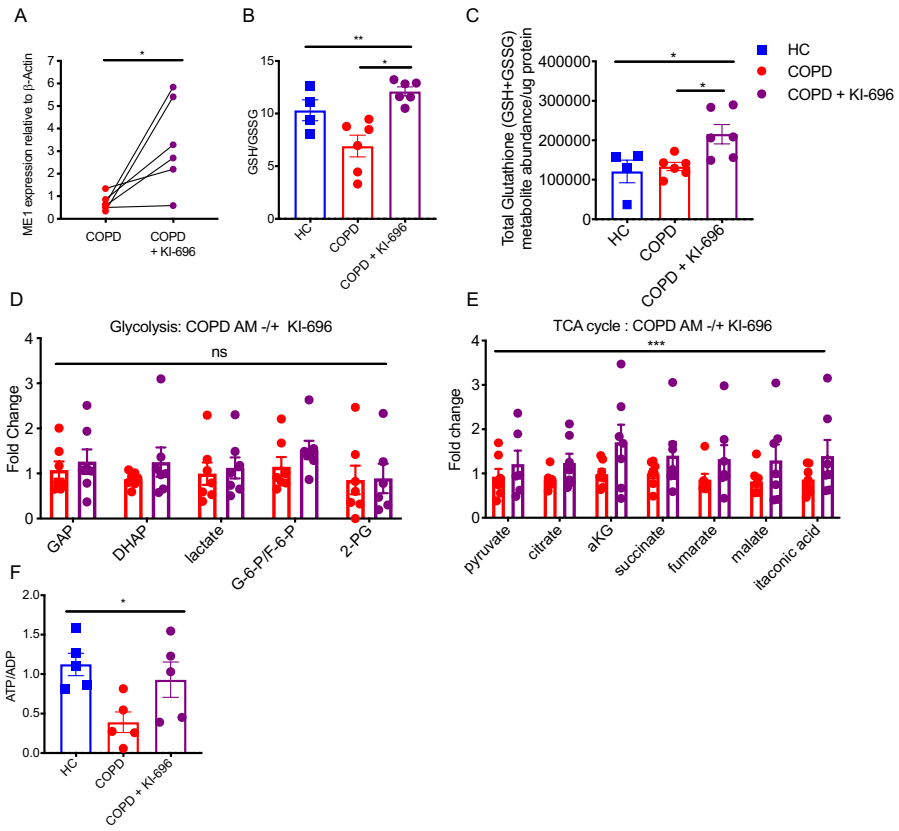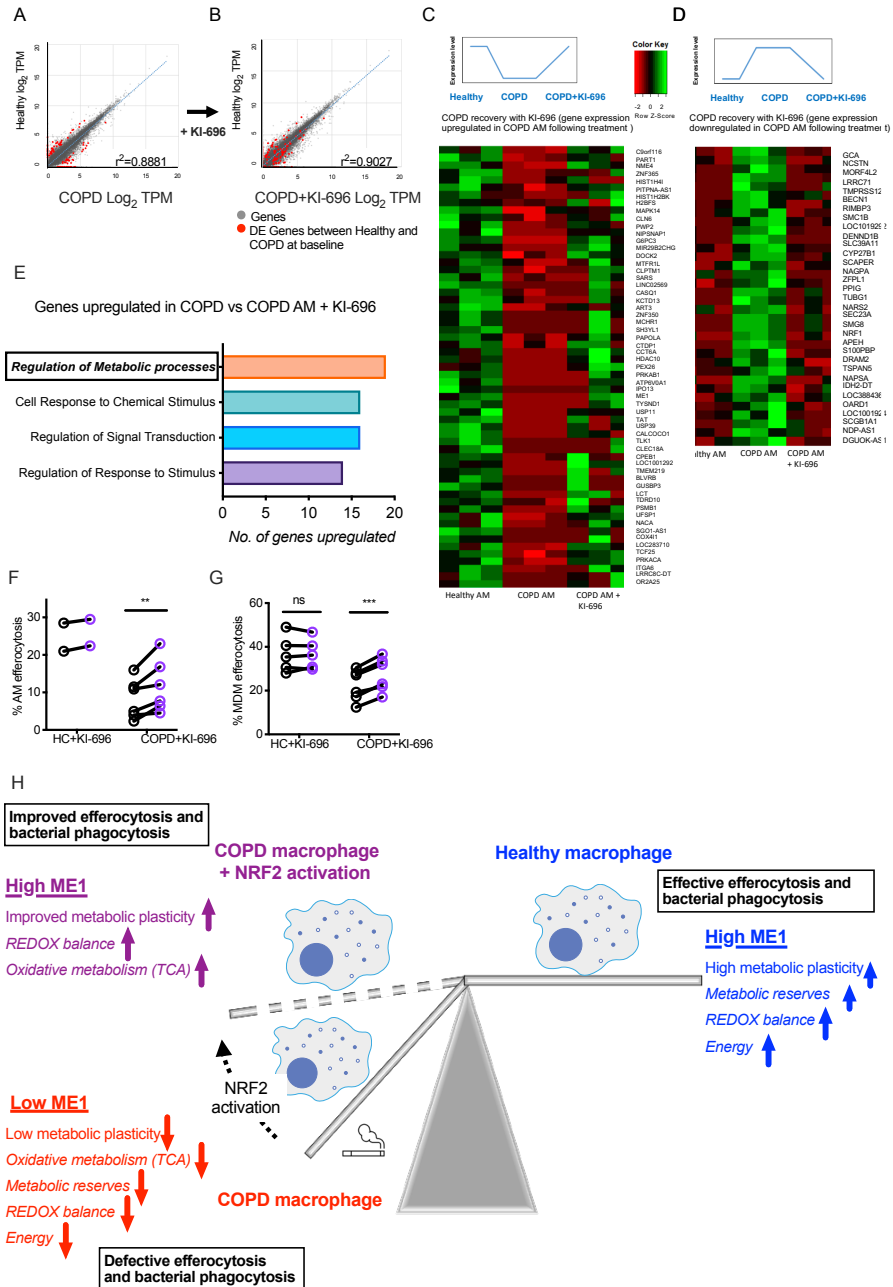
Figure 2:

Figure 3:

Figure 4:

Figure 5:

Figure 6:

Online Data Supplement:

NRF2 activation reprogrammes defects in oxidative metabolism to restore macrophage function in COPD

Authors: Eilise M. Ryan[1], Pranvera Sadiku[1], Patricia Coelho[1,] Emily R. Watts[1], Ailiang Zhang[1], Andrew J.M. Howden[2], Manuel A. Sanchez-Garcia[1], Martin Bewley[3], Joby Cole[3], Brian J. McHugh[1], Wesley Vermaelen[4], Bart Ghesquiere[4], Peter Carmeliet[5,6,7], Giovanny Rodriguez Blanco[8], Alex Von Kriegsheim[8], Yolanda Sanchez[9], William Rumsey[9], James F. Callahan[9], George Cooper[1], Nicholas Parkinson[10], Kenneth Baillie[10], Doreen A. Cantrell[2], John McCafferty[11], Gourab Choudhury[11], Dave Singh[12], David H. Dockrell[1], Moira K.B. Whyte[1]*†, Sarah R. Walmsley[1]*†.

Supplementary materials and methods:

Study Approval: Written informed consent was obtained and patients were recruited for bronchoscopy and venesection in accordance with local ethics (South East Scotland Research Committee , REC Ref 15/SS/0095 Greater Manchester South Rec ref 06/Q1403/156). Written informed consent was obtained from healthy volunteers for blood donation via the CIR Blood Resource Management Committee (AMREC 15-HV-013) in Edinburgh.

Patient recruitment: Patients were recruited for bronchoscopy and venesection in accordance with local ethics. COPD donors had an FEV1/FVC ratio of <0.70 , GOLD Stage 1,2,3 or 4 disease and were current or ex-smokers. Health status was evaluated via the validated COPD Assessment Test (E1). Healthy Bronchoscopy Donors (including "healthy smokers") had normal spirometry and were never, ex or current smokers. Patient demographics are outlined in Table 1. Patients were exacerbation free for at least 8 weeks and patients with diabetes, renal failure, liver failure, cardiac failure, active malignancy or other major respiratory diagnosis e.g. asthma/bronchiectasis were excluded. Patient samples were not randomized, but investigators were blinded to experimental conditions. Healthy volunteers for blood donation were age matched +/- 8 years .

Bronchoscopy: Bronchoalveolar Fluid (BAL) was collected from COPD and Healthy donors, as per ethics protocol. After inspection of the airways during bronchoscopy, the scope was wedged into the Right Middle Lobe (RML). 2-4 ml of lidocaine was then instilled via the scope into the RML, prior to injecting a total of 240ml of saline in 40ml

aliquots. The first 40ml of return was discarded/sent for routine culture and sensitivity, due to the high content of epithelial cells.

Seahorse Assays: After removal from standard culture plates, cells were seeded directly in to Xe24 seahorse assay plates (Agilent) at a density of 250,000 in 300 μl of monocyte-derived macrophages (MDM) and 210,000 in 300 μl per well of alveolar macrophages (AM) for 45 min at room temperature, before an additional 200 μl of complete medium was added to each well. All cells were subjected to either/both a glycolytic and mitochondrial stress test depending on cell numbers. For both Mitochondrial and Glycolytic stress test, 30ml of medium was made and pH adjusted as per the manufacturers guidelines (Agilent). Standard culture medium was replaced with 500μl of the appropriate Seahorse Stress Test Medium before incubating the plate at 37°C, with no CO_2 for 45 min. Glucose, Oligomycin , 2DG , FCCP and Antimycin & Rotenone were prepared as detailed below. Following the injection of each compound, three readings were taken 8 min apart totalling 3 cycles x 24 min each. Basal Glycolysis, Maximal Glycolytic Rate and Glycolytic Reserve (Glycolytic Stress Test) or Basal Oxygen Consumption, Maximal Respiratory Capacity, Spare Respiratory Capacity and Proton Leak (Mitochondrial Stress Test) were calculated during the assay and exported to Excel for analysis via Wave software (Agilent). ECAR & OCR readings were then normalised to μg protein/ml using a Pierce BCA assay (Thermo Scientific). When used, macrophages were co incubated with 20hr apoptotic neutrophils at an MOI of 10:1(healthy donors) and 15:2 (COPD donors) for 90min prior to vigorous washing for removal of any non-internalised neutrophils. In a separate experiment, to explore the nature of the increase in Spare Respiratory Capacity following co -incubation with

apoptotic neutrophils, healthy AM were co incubated with apoptotic neutrophils or pre-treated with known M2 stimuli (E2,E3). Cells were pre-treated with 20ng/ml IL-4 (68-8780-63, eBioscience) and 20ng/ml IL-13 (571102, BioLegend) or 20ng/ml IL-10 (217-IL, R&D) for 16hrs prior to running seahorse assays.

Glycolytic Stress Test	*Amount of media added to vial:*
Vial 1 : Glucose	3000µl
Vial 2: Oligomycin	720µl
Vial 3 : 2DG	3000µl
Mitochondrial Stress Test	
Vial 1: Oligomycin	630µl. Then 225µl of vial was added to 1.275ml media.
Vial 2:FCCP	720µl. Then 300µl of vial added to 1.275ml media.
Vial 3: Rotenone & Antimycin	540µl. Then 300µl of vial added to 1.2ml media.

RNA isolation and quantification: RNA was isolated from macrophages (approximately 600,000 cells per sample) or THP-1 cells (approximately $1x10^6$ cells per sample) using the mirVana total RNA isolation protocol (Ambion, Thermo Fisher),

DNase treated and reverse transcribed using AMV reverse transcriptase with random primers (Promega). Gene expression was analyzed using predesigned qPCR Primer/Probe assays and Prime Time Gene Expression Mastermix (IDT). Genes of interest were normalized to β actin expression.

Transcriptomic Analysis: *(A)* *COPD AM +/- KI-696 vs healthy AM +/- KI-696 data set:* RNA was extracted from Alveolar Macrophages and Total RNA-Sequencing performed by the Edinburgh Clinical Research Facility Genomics Core, Edinburgh UK. Analysis was performed by Thomson Bioinformatics as detailed :FastQ files were mapped to the reference genome (UCSC hg19) using the STAR alignment tool (STAR 2.6.1a) with filters applied allowing no more than 5 mismatches per read, read QC scores above a defined normalized threshold score of 0.66 and multimapping alignment scores no greater than 1. Following mapping overall metrics were analyzed to assess the quality of each run (i.e. % reads passing QC thresholds following removal of abundant RNA reads, median coverage uniformity statistics and comparative genomic alignment distribution analyses). Transcripts Per Million (TPM) scores were calculated for each gene across all samples. Differentially expressed (DE) genes were defined as genes displaying greater than Log_2 1.5 fold change and with P-values <0.05 between two sample cohorts.(E4,E5,E6).

(B) COPD AM and Healthy Donor AM +/- *S. pneumoniae*: This data set was previously published by our group, with details outlined in the manuscript (E6). In brief , AM from Healthy and COPD donors were co-incubated with *D39 Streptococcus pneumoniae* for 6 hours before vigorous washing .RNA was then extracted and hybridized onto the Affymetrix HG-U133 plus 2.0 Array. The transcriptomic data is available online in the

ArrayExpress database at EMBL-EAI www.ebi.ac.uk/arrayexpress, under accession

number EMTAB-6491. This data set was then independently re analysed by our lab

group, specifically targeting metabolism-related changes in transcription.

HPLC-MS analysis of metabolite abundance: Samples were generated by harvesting

approximately 600,000 AM, using 300μl of Methanol per sample, on ice. Samples were

stored for at least 24 hours in -80 C before being thawed on ice and spun at 10,000G

for 10 min at 4°C. Supernatant was removed for analysis using Dionex UltiMate 3000

LC System (Thermo Scientific) coupled to a Q Exactive Orbitrap mass spectrometer

(Thermo Scientific) operated in negative mode. Data collection was performed using

Xcalibur software (Thermo Scientific) verified by manual assessment of each sample

and metabolite. Samples were normalized to protein content by adding 200μl of 200 mM

NaOH to each pellet. Samples were then boiled at 95 C for 20min, cooled on ice and

spun down for 10min at 400G. Protein content was measured using a Pierce BCA

assay (Thermo Scientific). For 13C tracing experiments, differentiated THP-1 cells were

cultured in the presence of 5.5 mM U-13C glucose for 6 hours. Relative levels of

isotopologue abundance and 13C incorporation into lactate were measured as above

and compared to unlabelled (U-12C glucose) controls. Percentage labelling is

expressed as the percentage of 13C isotopologue of the total lactate abundance.

Generation of proteomic samples: Alveolar macrophages were isolated from BAL

fluid as detailed above and cultured for 3 days with daily washes prior to harvesting.

Cells were pelleted at 400G for 8 minutes , supernatant discarded and pellets flash

frozen. Protein extracts had the following added; SDS to a final concentration of 5%,

47

TCEP to a final concentration of 10mM and TEAB to a final concentration of 50mM. Samples were incubated at 95°C for 5 minutes before sonicating for 15 cycles of 30 seconds each using a BioRuptor (Diagenode). Proteins were alkylated in the dark for 1 hour by the addition of IAA at 20mM. Protein lysates were prepared for mass spectrometry using s-trap mini columns according to the manufactures instructions (Protifi). In summary, for each sample 200 mg of protein was loaded onto a s-trap mini column. Captured protein was washed 5 times with 400 ml of wash buffer (90% methanol with 100 mM TEAB, pH 7.1). Proteins were digested by the addition of 10 mg of trypsin to each sample in 50 mM ammonium bicarbonate. Samples were digested for 2 hours at 47 °C. Once digestion was complete, peptides were eluted with 80 ml of 50 mM ammonium bicarbonate followed by 80 ml of 0.2 % formic acid and lastly with the addition of 80 ml 50 % acetonitrile with 0.2 % formic acid. After the addition of each elution buffer, columns were centrifuged at 4000 g for 1 minute and the flow through collected. Eluted peptides were dried by speedvac and suspended in 1 % formic acid before quantification using the CBQCA assay (Invitrogen).

Proteomic Mass spectrometry analysis: For each sample 1.5 mg of peptide was analysed by data independent acquisition (DIA). Peptides were injected onto a nanoscale C18 reverse-phase chromatography system (UltiMate 3000 RSLC nano, Thermo Scientific) and electrosprayed into an Orbitrap Exploris 480 Mass Spectrometer (Thermo Fisher). For liquid chromatography the following buffers were used: buffer A (0.1% formic acid in Milli-Q water (v/v)) and buffer B (80% acetonitrile and 0.1% formic acid in Milli-Q water (v/v). Samples were loaded at 10 μL/min onto a trap column (100 μm × 2 cm, PepMap nanoViper C18 column, 5 μm, 100 Å, Thermo Scientific)

equilibrated in 0.1% trifluoroacetic acid (TFA). The trap column was washed for 3 min at the same flow rate with 0.1% TFA then switched in-line with a Thermo Scientific, resolving C18 column (75 μm × 50 cm, PepMap RSLC C18 column, 2 μm, 100 Å). Peptides were eluted from the column at a constant flow rate of 300 nl/min with a linear gradient from 3% buffer B to 6% buffer B in 5 min, then from 6% buffer B to 35% buffer B in 115 min, and finally to 80% buffer B within 7 min. The column was then washed with 80% buffer B for 4 min and re-equilibrated in 3% buffer B for 15 min. Two blanks were run between each sample to reduce carry-over. The column was kept at a constant temperature of 50°C. The data was acquired using an easy spray source operated in positive mode with spray voltage at 2.445 kV, and the ion transfer tube temperature at 250oC. The MS was operated in DIA mode. A scan cycle comprised a full MS scan (m/z range from 350-1650), with RF lens at 40%, AGC target set to custom, normalised AGC target at 300%, maximum injection time mode set to custom, maximum injection time at 20 ms, microscan set to 1 and source fragmentation disabled. MS survey scan was followed by MS/MS DIA scan events using the following parameters: multiplex ions set to false, collision energy mode set to stepped, collision energy type set to normalized, HCD collision energies set to 25.5, 27 and 30%, orbitrap resolution 30000, first mass 200, RF lens 40%, AGC target set to custom, normalized AGC target 3000%, microscan set to 1 and maximum injection time 55 ms. Data for both MS scan and MS/MS DIA scan events were acquired in profile mode.

Analysis of proteomic DIA-MS data: Raw mass spec data files were searched using Spectronaut (Biognosys) version 16.0.220606.53000 using the directDIA function. The following search settings were used: minimum peptide length 7, maximum peptide

length 52, cleavage enzyme Trypsin, maximum missed cleavages 2, protein and

peptide FDR was set at 0.01, profiling and cross run normalisation were disabled.

Carbamidomethyl (C) was selected as a fixed modification while Acetyl (N-term),

Deamidation (NQ) and Oxidation (M) were selected as variable modifications. Data

were searched against a human database with isoforms from Uniprot release 2021 01.

Estimated protein copy numbers and concentration were calculated using the proteomic

ruler (E7) and Perseus (E8). The normalized intensity for each identified protein was

calculated by dividing the individual protein intensity by the total intensity obtained per

sample to correct for technical variances during data acquisition between samples, prior

to determining significance on Peresus .

Immunostaining for microscopy: Health and COPD patient lung sections were

prepared from paraffin-embedded blocks. The lung sections were stained with anti-

CD68 (ab201340, Abcam), anti-ME1 (ab223761, Abcam) after deparaffinization and

antigen retrieval. The following were used- TSA plus system amplification

(NEL744B001KT, Perkin Elmer) and autofluorescence quenching with TrueView

(Vector, SP-8400). The nuclei were stained with DAPI (422801, Sigma-Aldrich). Images

were acquired using a Leica SP8 confocal microscope at 20x magnification.

ME1 **knockout in THP-1 cells**: CRISPR-Cas9 mutagenesis was used to create a

polyclonal population of *ME1*-null THP-1 cells. First, a protospacer sequence encoding

a single guide RNA targeting the protein-coding sequence in the first exon of *ME1* (5'

ATGGGTGTGGCGGCGACGGG-3') was cloned into LentiCRISPRv2 (a gift from Feng

Zhang; Addgene plasmid #52961) according to previously described protocol (E9). The

vector was packaged into lentivirus using the LV-Max Lentiviral Production System (Gibco) according to the manufacturer's instructions. THP-1 cells were transduced, at a multiplicity of infection of approximately 1, by spin infection at 1000g for 1 hour at 32°C. Puromycin was added to the medium after 48 hours, and the cells were cultured under puromycin selection for 7 days.

ME1 chemical inhibition of monocyte-derived macrophages: Healthy MDM were pre-treated with a chemical ME1 inhibitor (Medchem HY-124861) at 100µM or DMSO vehicle control for 16 hours prior to running a mitochondrial stress test on Seahorse to determine basal OCR:ECAR rates, as described above. To determine the effect of ME1 inhibition on basal mROS production , healthy MDM at day 12-14 of culture were transferred to iBidi 8-well chamber slides and subsequently treated for 16hrs with 100µM ME1 inhibitor or DMSO vehicle control. To detect mitochondrial ROS, MDMs were washed x2 in warm HBSS, and incubated with 2µM MitoSox Red reagent (Thermo Fisher Scientific) in warm phenol red-free RPMI for 20 minutes at 37°C. Cells were then washed again x2 in HBSS, and imaged immediately using an Andor spinning disk confocal microscope 60x objective, 0.5µM intervals at 610nm wavelength. Z-stack images were processed in Imaris software, and mean fluorescence intensity of MitoSox Red was obtained from >180 cells per condition from a total of 3 different donors.

GSH:GSSG Quantification: Samples were generated using 2 x 10^6 cells of THP-1 EV and THP-1 *ME1* KO cells. GSH:GSSG µmol/l was determined via a colorimetric assay,

as per the manufacturer's protocol (Sigma-Aldrich 38185). A 1in 4 dilution was used for calculating GSH concentration.

mtDNA:nDNA content: 2 ng of DNA extracted using DNeasy Blood & Tissue Kit (QIAGEN) were subjected to qPCR using primers for mitochondrial DNA (mtDNA) mtF3212 (5'CACCCAAGAACAGGGTTTGT3'), mtR3319 (5'TGGCCATGGGTATGTTGTTAA3') and for nuclear DNA (nDNA) 18SrRNA gene 18S1546F (5'TAGAGGGACAAGTGGCGTTC3'), 18S1650R (5'CGCTGAGCCAGTCAGTGT3'). The probes used were 5'6-FAM/ZEN-TTACCGGGCTCTGCCATCT 3'IBFQ and 5' HEX-AGCAATAACAGGTCTCTGATG 3' BHQ®-2 for mtDNA and nDNA, respectively.

NRF2 activation via KI-696: Alveolar and monocyte-derived macrophages or THP-1 *ME1* KO cells were treated for 16 hours with the highly specific NRF2 activator, KI-696 at 0.065 µM ,provided by GSK (E10). Cells were then washed and harvested for RNA isolation (Fig. 5A ,Fig. 6A-E) , assessment of metabolite abundance via HPLC-MS (Fig. 5 B-F) or co-incubated with PKH26 labelled 20h apoptotic neutrophils and run on flow cytometry (Fig. 6 F-G , fig. E6E), as described in the main manuscript materials and methods. To assess if NRF2 mediated rescue of COPD macrophage required sustained presence of KI-696, COPD MDM were (A) treated for 16 hours with KI-696 at then washed and rested for a further 16 hours prior to co-incubation with PKH26 labelled 20 hour apoptotic neutrophils or (B) treated for 16 hours with KI-696 then washed and immediately co-incubated with apoptotic neutrophils for assessment on flow cytometry (fig E6D).

Bronchoalveolar fluid assessment: Aliquots of Bronchoalveolar Lavage Fluid were generated during the isolation of alveolar macrophages as described above. All nutrient concentrations were determined using fluorometric/colorimetric plate-based assays, as per the manufacturer's protocol and the optimal dilution of samples was ascertained for each different analyte. Concentrations used were: Glucose (Biovision K606-100): 1in2 dilution, 10 minute incubation; Glutamine (Abcam 197011) 1in2 dilution, 60 minute incubation; Lactate (Abcam 65330) 1in2 dilution, 30 minute incubation, prior to measuring nutrient concentration.

Determining intracellular glycogen concentrations : Glycogen stores were measured in both Monocyte-Derived Macrophages (MDM) and Alveolar Macrophages (AM). Three wells of approximately 200,000 cells per well were combined per condition. Wells were rapidly washed with cold PBS on ice x 3 to remove media then scraped in 200μl H$_2$0 per well. Lysates were boiled at 100°C for 10 min then spun at 13,000G for 5 min at 4°C. The supernatant glycogen content was determined via a fluorometric plate based assay (Sigma-Aldrich MAK016-1KT) at a 1:2 dilution, as per the manufacturer's guidelines. The cell pellet was stored for protein quantification and consequent glycogen content protein normalisation, via a Pierce BCA assay (Thermo Scientific).

Measuring Glucose uptake via a 2NBDG Assay: Uptake of 2NBDG was measured as a surrogate for glucose uptake using a 2NBDG kit (Cayman Chemical 600470). Cells were incubated in glucose free medium (Gibco, 11879-020) for 90min. 250μl of 240 μM proprietary glucose was added to each well for 60 min before adding the Cell Based assay buffer and incubation on ice for 10 min. Supernatant was aspirated and 100μl of

1:100 Infra-Red Fixed viability (Biolegend,423195) stain was added, incubated for 10 minutes, light protected, on a shaking platform. 200μl of cell Based Assay buffer was then added and the TC plate was incubated on ice for 10 min prior to analysis on an Attune NXT flow cytometer. Control wells were pre-treated for 24 hours with Apigenin (included in the kit) to inhibit 2NBDG uptake.

Supplementary References :

E1.Gupta N, Pinto LM, Morogan A, Bourbeau J. The COPD assessment test: a systematic review. *Eur Respir J.* 2014;44(4):873-884.

E2.Jha AK, Huang SC-C, Sergushichev A, et al. Network integration of parallel metabolic and transcriptional data reveals metabolic modules that regulate macrophage polarization. *Immunity.* 2015;42(3):419-430. doi:10.1016/j.immuni.2015.02.005.

E3.Zhang S, Weinberg S, DeBerge M, et al. Efferocytosis Fuels Requirements of Fatty Acid Oxidation and the Electron Transport Chain to Polarize Macrophages for Tissue Repair. *Cell Metabolism.* 2019;29(2):443-456.e445. doi:10.1016/j.cmet.2018.12.004.

E4.Smith LC, Venosa A, Gow AJ, Laskin JD, Laskin DL. Transcriptional profiling of lung macrophages during pulmonary injury induced by nitrogen mustard. Ann N Y Acad Sci. 2020 Nov;1480(1):146-154. doi: 10.1111/nyas.14444.

E5.Shen L, Zhou K, Liu H, Yang J, Huang S, Yu F, Huang D. Prediction of Mechanosensitive Genes in Vascular Endothelial Cells Under High Wall Shear Stress. Front Genet. 2022 Jan 11;12:796812. doi: 10.3389/fgene.2021.796812.

E6. Bewley MA, Budd RC, Ryan E, et al. Opsonic Phagocytosis in Chronic Obstructive Pulmonary Disease Is Enhanced by NRF2 Agonists. *Am J Respir Crit Care Med.* 2018;198(6):739-750.

E7.Wiśniewski JR, Hein MY, Cox J, Mann M. A "proteomic ruler" for protein copy number and concentration estimation without spike-in standards. Mol Cell Proteomics. 2014 Dec;13(12):3497-506. doi: 10.1074/mcp.M113.037309.

E8.Tyanova, S., Temu, T., Sinitcyn, P. *et al.* The Perseus computational platform for comprehensive analysis of (prote)omics data. *Nat Methods* **13**, 731–740 (2016). https://doi.org/10.1038/nmeth.3901

E9.Sanjana NE, Shalem O, Zhang F. Improved vectors and genome-wide libraries for CRISPR screening. *Nat Methods*. 2014;11(8):783-784.

E10. Davies TG, Wixted WE, Coyle JE, et al. Monoacidic Inhibitors of the Kelch-like ECH-Associated Protein 1: Nuclear Factor Erythroid 2-Related Factor 2 (KEAP1:NRF2) Protein-Protein Interaction with High Cell Potency Identified by Fragment-Based Discovery. *J Med Chem*. 2016;59(8):3991-4006. doi:10.1021/acs.jmedchem.6b00228

Supplementary Figures:

Figure E1. Age does not influence macrophage phagocytosis and efferocytosis.

Figure E2. COPD macrophages display equivalent basal metabolic rates coupled with a loss of metabolic plasticity, that is not attributable to a polarisation state.

Figure E3. Substrate availability and mitochondrial function does not differ between COPD and healthy donors.

Figure E4. Transcript expression of *ME1* in control and *ME1* knockout THP-1 cells.

Figure E5. Survey of proteomic markers does not support a senescence switch in COPD AM.

Figure E6. Protein abundance of NRF2 dependent and independent scavenger markers is reduced in COPD. NRF2 mediated pharmacological rescue of efferocytosis in COPD MDM requires sustained presence of the NRF2 agonist, KI-696, and the presence of ME1.

Figure E1. Age does not influence macrophage phagocytosis and efferocytosis.

Correlation of bacterial internalization rates (A, n=19) and efferocytosis rates (B, n=28) with macrophage donor age. Data represents individual values. Pearson's correlation coefficient (r) and p values shown.

Figure E2. COPD macrophages display equivalent basal metabolic rates coupled with a loss of metabolic plasticity, that is not attributable to a polarisation state.

(A-D) Glycolytic (A,C) and mitochondrial (B,D) stress testing was performed in COPD (circles) and healthy (squares) donor AM and MDM (A, HC n=6, COPD n=10, B HC n=9, COPD n=12; C, n=5) D, n=7) Open symbols represent current smokers. COPD Smoker vs Ex-smoker, (A) P value=0.06, (B) P value= 0.41, (C) P value= 0.09. **(E-F)** Healthy and COPD donor macrophages were co incubated for 90 min with 20 h apoptotic neutrophils (+AN) prior to performing assays. Spare respiratory capacity (E, HC n=8, COPD n=6) and glycolytic reserve (F, HC n=5, COPD n=3) were determined by Seahorse analysis. (G) Healthy Donor AM were co incubated with 20h apoptotic neutrophils or treated for 16h with M2 polarizing stimuli 20ng/ml IL-10 or IL-4&13 (n=3). **(H)** Protein abundance of M1 and M2 Markers , as detected by data-independent acquisition MS proteomic analysis , in COPD relative to Healthy Non Smoker AM (diamonds) and COPD relative to "Healthy Smoker" AM (triangles). COPD AM n= 7, HNS and HS n= 5. Data represents individual values and mean ± SEM. Significance was determined by (A,B,D) unpaired t-test, (C) Mann-Whitney U Test, (E, F, G) two-way

ANOVA with Tukey's multiple comparisons. *P ≤0.05. ns= not significant . Apoptotic

Neutrophil (AN) MOI=10:2 Healthy AM; MOI 15:2 COPD AM.

Figure E3. Substrate availability and mitochondrial function does not differ

between COPD and healthy donors. (A) Relative protein abundance of mitochondrial

fusion and fission proteins in COPD AM relative to Healthy Non-Smoker (HNS) and

"Healthy Smoker" (HS) AM. COPD AM n= 7, HNS and HS n= 5. Protein abundance

measured by data-independent acquisition MS proteomic analysis. **(B-D)** Colorimetric

assays were used to determine glutamine (B, HC n=9, COPD n=8), Glucose (C, HC

n=8, COPD n=9) and lactate concentration (D, n=8) in Bronchoalveolar Lavage (BAL)

fluid from COPD (circles) and healthy(squares) donors. **(E)** Glucose uptake was

measured in MDM via a 2-NBDG assay and analysed via flow cytometry, n=7. Uptake

rates were normalised to median cell fluorescence of unstained cells. **(F-G)**The fold

change increase in ECAR rates following glucose injection was calculated for healthy

and COPD AM (E, HC n=5, COPD n=7) and MDM (F, n=5, No Glucose [NG] conditions

n=4). Prior glucose deprivation for 16h was used as a positive control. **(H)** Glycogen

abundance was measured in healthy (n=5) and COPD (n=6) AM and MDM using a

colorimetric assay. Data represents individual values and mean ± SEM. P values

calculated by (A) 2-way ANOVA with Tukey's multiple comparisons. (B-E) unpaired t-

test and (F,H) Mann Whitney U test, (G) Kruskal Wallis test with Dunn's multiple

comparisons. * P ≤0.05, **P ≤0.01, ns= not significant. MFI= Median Fluorescence

Intensity, FMO =Fluorescence minus one, unstained cells. NG= No Glucose.

Figure E4. Transcript expression of malic enzyme1 (ME1) in control and *ME1* knockout THP-1 cells. *ME1* was deleted in the THP1 macrophage cell line using CRISPR cas9 mutagenesis. Control (EV) and *ME1* knockout (ME1 KO) THP1 cells were lysed and qPCR analysis of cDNA performed with data normalized to β- Actin (ACTB) expression, n= 3. Data represents individual values and mean ± SEM. P value calculated by paired t-test.

Figure E5. Survey of proteomic markers does not support a senescence switch in COPD AM. (A-F) Relative protein abundance in COPD, Healthy non-smoker (HNS) and "Healthy Smoker" (HS) AM of detected makers of senescence. COPD AM n= 7, HNS and HS n= 5. Protein abundance determined by data-acquisition independent MS proteomic analysis. Data represents individual values and mean ± SEM. P values calculated by (A-D) Kruskal-Wallis test with Dunn's multiple comparisons. * P ≤0.05, ns= not significant.

Figure E6. Protein abundance of NRF2 dependent and independent scavenger markers is reduced in COPD. NRF2 mediated pharmacological rescue of efferocytosis in COPD MDM requires sustained presence of the NRF2 agonist, KI-696, and the presence of ME1. (A-C) Protein abundance of the NRF2 dependent (MARCO) and NRF2 independent scavenger receptors (SRA1 and SRA6) is reduced in COPD AM relative to Healthy Non/Smoker AM (HNS,HS). COPD n= 7, HNS and HS n=5. Protein abundance was measured by data-independent acquisition MS proteomic analysis. **(D)** COPD MDM were treated for 16 hours with KI-696 or treated with KI-696 for 16 hours then washed and rested for 16 hours (KI-696 wash off) prior to co-incubation with PKH26 labelled 20h apoptotic neutrophils, n=4. **(E)** *ME1* knockout (*ME1*

KO) THP1 macrophage cells were incubated for 16 hours in the presence or absence of KI-696 prior to co-incubation with PKH26 labelled 20h apoptotic neutrophils, n=7. Efferocytosis rates were measured via flow cytometry. Data represents individual values and mean ± SEM. P values calculated by (A-C) Kruskal-Wallis test with Dunn's multiple comparisons, (D) 2-way ANOVA with Dunnet's multiple comparisons and (E) paired t-test. * P ≤0.05, **P ≤0.01, ns= not significant.
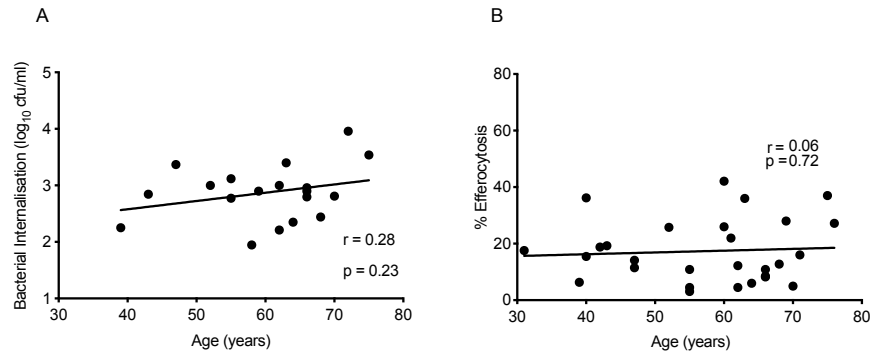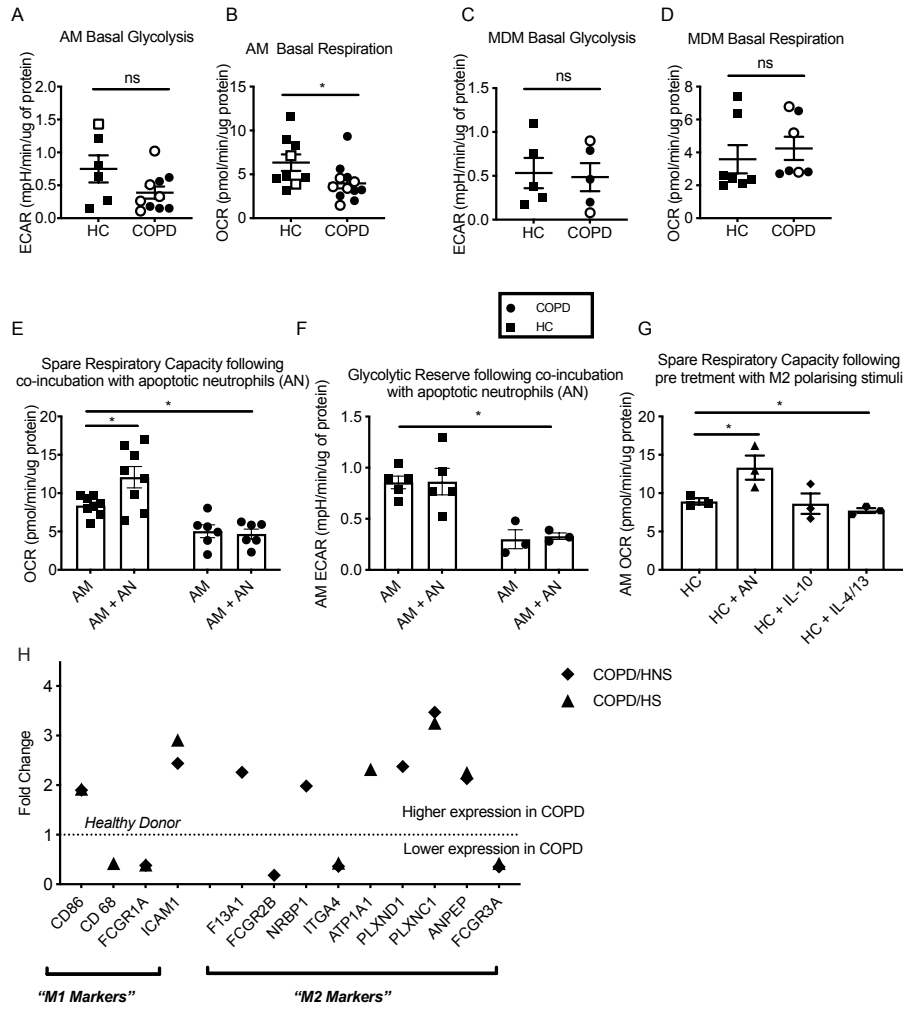
A

Bacterial Internalisation (log$_{10}$ cfu/ml)

Age (years)

r = 0.28
p = 0.23

B

% Efferocytosis

Age (years)

r = 0.06
p = 0.72

Figure E1:

Figure E2:

A Mitochondrial Fussion and Fission AM

B

C

D

E MDM 2-NBDG uptake

F AM ECAR following glucose Injection
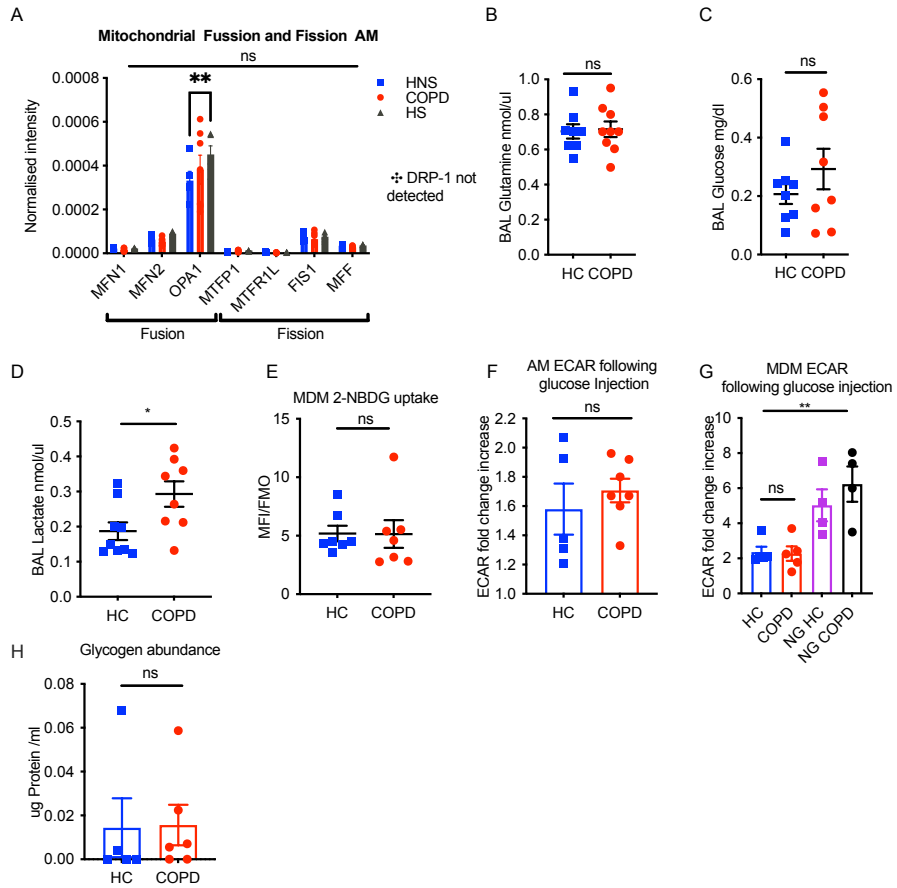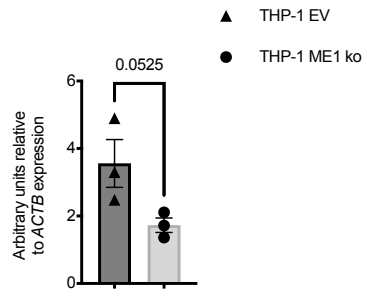
G MDM ECAR following glucose injection

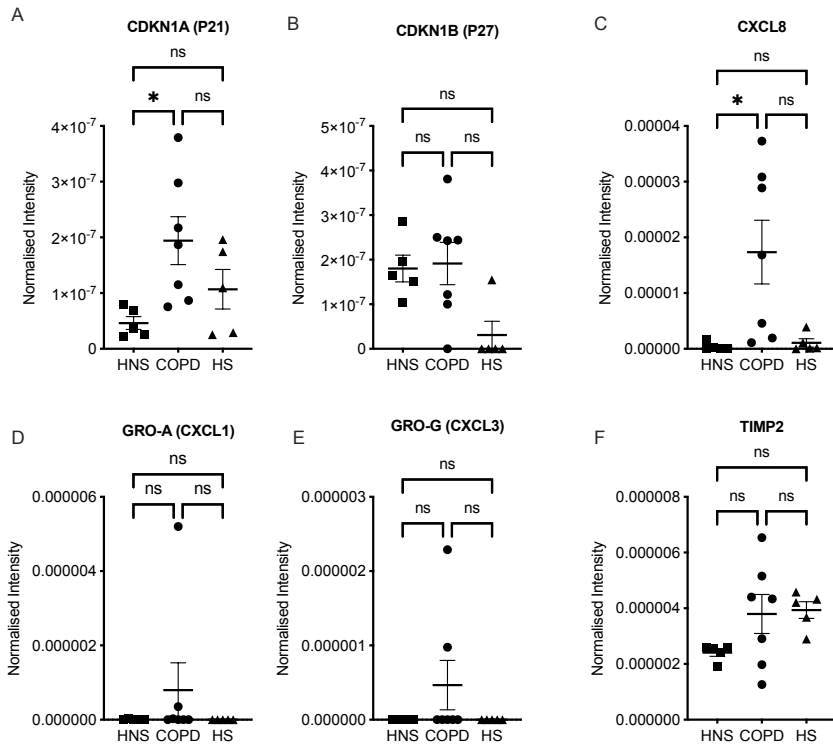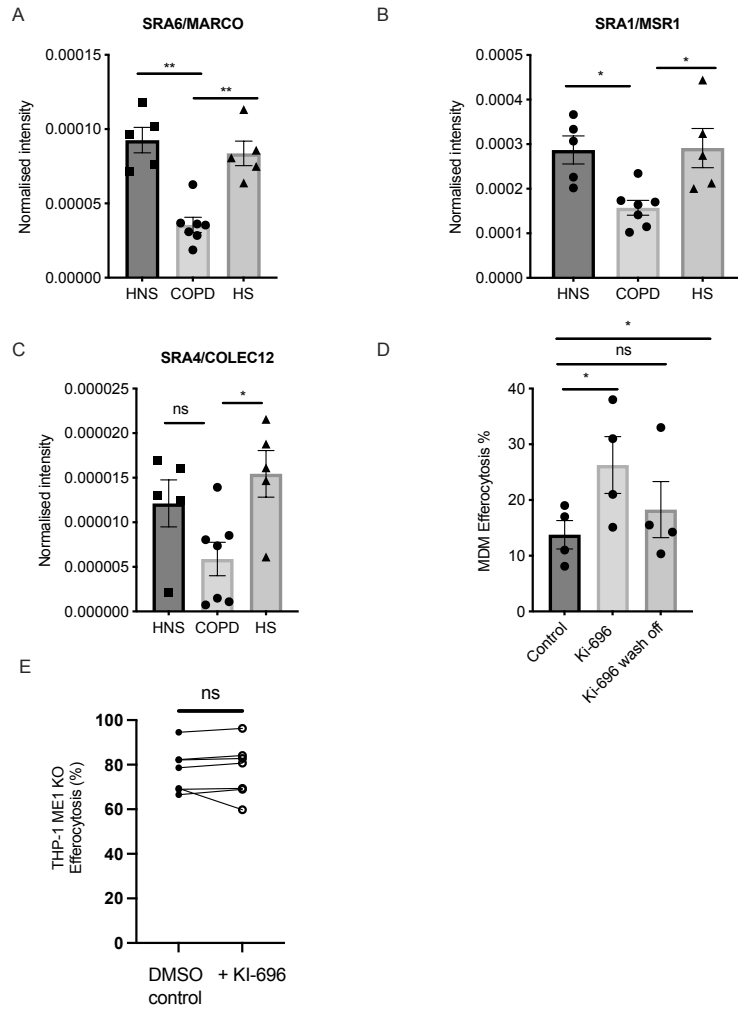**H** Glycogen abundance

Figure E3:

Figure E4:

Figure E5:

Figure E6: